

STRUCTURAL AND CHEMICAL EVOLUTION OF LOW- AND INTERMEDIATE-MASS STARS

Lionel Siess¹

Abstract. We review the structural and nucleosynthetic evolution of stars in the mass range $0.8 - 11 M_{\odot}$, focusing on the AGB and super-AGB phases. The effects of transport processes associated with rotation and overshooting are described and their impact on nucleosynthesis analyzed. We present selected observational properties of AGB stars and discuss the weaknesses and failures of current stellar modeling.

1 Evolution up to the AGB phase

The evolution of stars is principally determined by their initial mass and, to a lower extent, by their composition and by the presence or not of mixing processes. Stars typically less massive than $0.5 M_{\odot}$ are unable to develop temperatures high enough to ignite helium and terminate their evolution as degenerate He white dwarf. Stars above that critical mass and below $\sim 2 - 2.5 M_{\odot}$ develop degenerate cores and ignite helium off-center “explosively” during the so-called He-flash. Such stars belong to the group of low-mass stars which differ from intermediate-mass stars ($2 - 2.5 M_{\odot} \lesssim M_{\text{ini}} \lesssim 6 - 8 M_{\odot}$) by the fact that the latter ignite He quietly at the center. Above $10 - 13 M_{\odot}$ (depending on the metallicity and on the treatment of convective mixing), the stars evolve through all nuclear burning stages (C, Ne, O and Si burnings) up to the formation of an iron core : this is the realm of massive stars. In a narrow mass range between $6 - 8 M_{\odot}$ and $10 - 13 M_{\odot}$ a very specific class of objects exists, named super-AGB stars, that complete central carbon burning but do not proceed any further.

The main topic of this chapter is to review the structural and chemical evolution of stars between ~ 0.5 and $10 - 13 M_{\odot}$ beyond central H-burning.

¹ Institut d’Astronomie et d’Astrophysique, Université Libre de Bruxelles, CP 226, B-1050 Brussels, Belgium

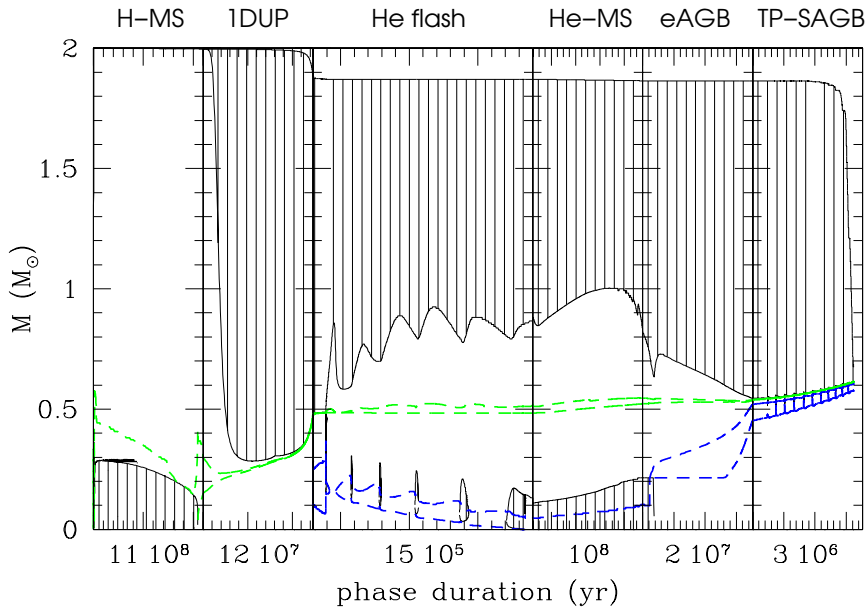


Fig. 1. Evolution of the internal structure of a $2 M_{\odot}$ star of solar metallicity. The successive panels correspond to the main sequence (H-MS), RGB phase characterized by the appearance of the first dredge-up (1DUP), helium flash and central helium burning (He-MS), *Early AGB* and thermally pulsing AGB (TP-AGB) phases. The regions of nuclear energy production due to H and He burning are also indicated by the dashed lines. The numbers on the x-axis represent the duration (in yr) of each evolutionary phase.

1.1 The sub-giant branch

When hydrogen is depleted at the stellar center, the nuclear energy production drops and the convective core, if present, disappears. The star contracts and the H-rich material surrounding the core moves inward and eventually ignites in a thick shell (Fig. 1). Most of the energy from the hydrogen-burning shell (HBS) is used to push matter away in both directions. This thick shell phase continues until the core mass reaches $\simeq 10\%$ of the stellar mass which corresponds to the Schönberg-Chandrasekhar limit. Beyond this limit, the core undergoes a strong contraction, the nuclear energy production increases and the HBS narrows. During this phase, the decrease in the HBS mass is compensated by the increase in its temperature so the luminosity remains approximately constant. As the core contracts, the envelope expands and the star crosses the HR diagram almost horizontally through the *Hertzsprung gap* (Fig. 2). This transition between central and peripheral nuclear burning modes occurs on a Kelvin-Helmholtz timescale ($\sim 10^5$ yr for a $1 M_{\odot}$).

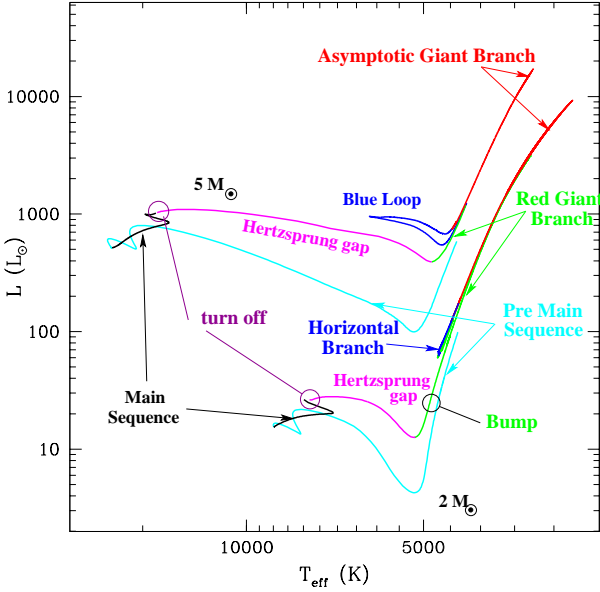


Fig. 2. Evolution in the HR diagram of a low- ($1 M_{\odot}$) and intermediate-mass ($5 M_{\odot}$) star. The evolutionary phases are also indicated : pre main-sequence (cyan), main sequence (black), the *Hertzsprung gap* (green), the RGB (magenta), central helium burning phase (blue) and the AGB phase (red).

1.2 The first dredge-up

The expansion of the star induces the cooling of the external layers. As the opacity increases near the surface, the transport of energy by radiation becomes less efficient and convection naturally develops. The convective zone grows in mass and moves inward during the so-called first *dredge-up* (1DUP). When the envelope reaches the layers where hydrogen was nuclearly processed (both during core and shell H burning), the products of proton burning are dredged-up to the surface. The 1DUP is responsible for the surface enrichment of ^4He and ^3He (produced by the cycle pp), of ^{13}C and ^{14}N (by-products of the CN cycle), for the dilution of the remaining ^7Li (partially burnt during the earlier pre-main sequence phase) and for a small decrease of the ^{12}C content. At its maximum extension, the envelope includes more than 70% of the stellar mass, which represents nearly 90% of the radius.

At this stage, the evolution of the primordial stars presents some interesting differences. Formed just after the big bang, these population III stars are characterized by a composition in which the metals and in particular of the CNO elements are absent. This peculiarity affects the evolution of low- and intermediate-mass stars. In particular, during the main sequence, stars more massive than $\sim 1 M_{\odot}$ cannot activate the CN cycle because of the absence of the catalytic seeds. As a consequence they contract until the central temperature reaches 10^8K and the 3α reactions ignite while the star is still on the main sequence. Thus, when hydrogen is exhausted in the core, helium burning reactions smoothly take over the nuclear energy production, without notable structural readjustment and the 1DUP is avoided. For lower mass stars that sustain their nuclear energy production by

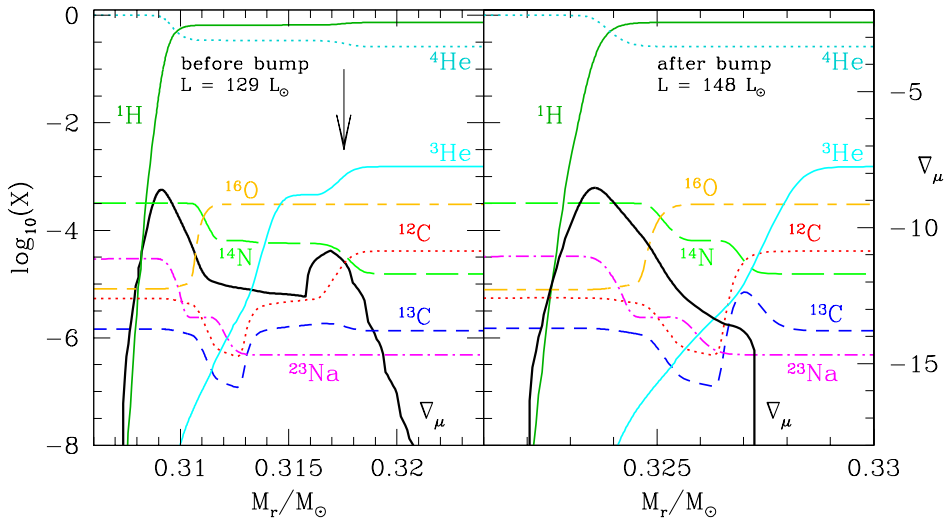


Fig. 3. Profiles of the main chemical species and gradient of mean molecular weight ($\nabla\mu$) in the vicinity of the HBS for a $0.85 M_{\odot}$ star with $Z = 0.0005$ before (left) and after (right-hand side) the passage of the *bump*. The stellar luminosity corresponding to these models is indicated in each panel. The HBS can be identified by the first (i.e., inner) peak in the μ gradient and the arrow indicates the position of the maximum inward extent of the convective envelope during the 1DUP. In the models before and after the *bump*, the base of the convective envelope is located at $M_r = 0.336$ and $M_r = 0.350 M_{\odot}$, respectively. These models corresponds to the standard case without extra-mixing (Palacios et al. 2006). In order to account for a decrease in the $^{12}\text{C}/^{13}\text{C}$ ratio after the *bump*, some extra-mixing must connect the base of the envelope with the ^{13}C peak located at $M_r \simeq 0.327 M_{\odot}$ (right panel). However, the origin of this extra-mixing is not clearly identified.

the pp chains ($M \lesssim 0.8 M_{\odot}$ at $Z = 0$), the 1DUP is present. However its effect is weak : a slight increase in the surface abundance of ^3He and ^4He and the dilution of remaining lithium.

1.3 The “bump” and the ascent of the red giant branch

As the star ascends the giant branch, the deepening of the envelope is slowed down by the increasing influence of the approaching HBS and eventually it reaches a maximum depth. When the envelope retreats, it leaves in its wake a chemically homogeneous zone which composition is different from that of the underlying radiative layers (which were previously affected by nuclear burning). At the mass coordinate corresponding to the deepest penetration of the envelope, a strong gradient of chemical composition ($\nabla\mu$) appears (Fig. 3) that prevents mixing to operate efficiently (see Suzanne Talon in this volume).

When the HBS crosses this “molecular weight barrier”, the nuclear energy

production is altered by the modification of the chemical composition. The luminosity of the giant star temporarily decreases due to the abrupt changes in the mean molecular weight and opacity. This structural readjustment, which only occurs in the lower mass stars that experience the helium flash ($M \lesssim 2.0 - 2.5 M_{\odot}$ according to the metallicity), makes the stars spend more time in this luminosity bin and observationally they accumulate in the HR diagram, whence the denomination of “*bump*” (Fig. 2). Thereafter, the HBS resumes its outward progression associated with the core growth and the internal temperature of the helium core increases. At the surface, the electrons recombine and the opacity, mainly due to H^{-} , decreases. The external layers become more transparent to radiation, the luminosity rises, the structure expands and the star climbs the red giant branch. During this ascent, the HBS narrows and the degeneracy of the slowly contracting core increases. The properties of the RGB stars are mainly determined by the He core mass and are practically independent of the envelope mass. As an illustration, the H-depleted core mass at helium ignition (Iben & Renzini 1984) is given by

$$M_{\text{core}} \simeq 0.476 - 0.221(Y - 0.3) - 0.009(3 + \log Z) - 0.023(M - 0.8) ,$$

where Y is the helium mass fraction, Z the metallicity¹ and M the stellar mass. We note the weak dependence of M_{core} on the mass for stars of a given chemical composition. As a consequence, the evolutionary tracks converge in the HR diagram and the central properties (density and temperature for example) are very similar among stars of initially different masses. During the RGB evolution, the mass loss increases substantially. Negligible on the main sequence, it can reach values as high as $\gtrsim 5 \times 10^{-7} M_{\odot} \text{ yr}^{-1}$ at the top of the RGB. Finally let us note that very low-mass stars ($M \lesssim 0.5 M_{\odot}$) or stars suffering abnormally large mass loss rate (e.g. because of the presence of a companion) will never ignite helium and will end their life as helium white dwarfs.

1.4 Mixing on the RGB

At the beginning of the RGB phase, the 1DUP modifies the surface chemical composition and brings additional constraints to stellar modeling. Various observations carried out on stars belonging to the Galaxy and/or to globular clusters indicate a systematic reduction in the $^{12}\text{C}/^{13}\text{C}$ ratio with luminosity, in agreement with the standard models until the *bump*. Beyond that point, for a magnitude $M_V < 2$, the carbon isotopic ratio abruptly decreases below its predicted value (≤ 15 instead of ~ 40) *in practically all observed stars*, independently of the environment. Based on a large sample of 108 stars located above the *bump*, Charbonnel & Do Nascimento (1998) showed that nearly 96% of them have a $^{12}\text{C}/^{13}\text{C}$ value significantly lower than the theoretical one. The same observation holds for lithium which destruction is enhanced after the *bump* in almost 100% of the

¹The metallicity Z is defined by $Z = 1 - X - Y$ where X and Y are the mass fractions of hydrogen ($^1\text{H} + ^2\text{H}$) and of helium ($^3\text{He} + ^4\text{He}$), respectively. The metallicity represents the mass fraction of metals, i.e. elements of charge > 2 .

cases (Gratton et al. 2000). The nitrogen abundance is more difficult to determine because of its molecular association in CN but an anti-correlation between carbon and nitrogen and the constancy of $(C+N+O)/Fe$ (Briley et al. 2004a) are also observed.

These observations tell us important things : (1) RGB stars experience non-standard mixing processes that alter the surface composition, (2) these processes are independent of the environment and metallicity, and (3) they take place at a very specific time of the evolution: at the *bump*. The mechanism allowing for the transport of the chemicals from the nuclear site of production to the envelope (Fig. 3) remains unknown. Different approaches using either parametric diffusion coefficients (Denissenkov & Weiss 1996; Denissenkov et al. 1998; Weiss et al. 2000) or different recipes for rotational mixing (Sweigart & Mengel 1979; Charbonnel 1995; Denissenkov & Tout 2000, 2003; Denissenkov & Vandenberg 2003) have been investigated and were somehow able to reproduce the observations. However all these studies were using more or less justified assumptions and initial conditions. A more consistent modeling considering the full treatment of rotational mixing from the main sequence to the top of the RGB showed that, in its present formulation, this mechanism is not able to reproduce the chemical anomalies observed at the *bump* in globular clusters (Palacios et al. 2006). The main reason is attributed to the fact that, by the time the HBS reaches the chemical discontinuity, angular momentum has been transported and the gradient of angular velocity significantly eroded. The shear being reduced, the diffusion process is largely inhibited and mixing is prevented. With the help of 3D hydrodynamical simulations of red giant stars Eggleton et al. (2006) identified a new mechanism that could be responsible for the development of extra-mixing at the *bump*. These authors showed that the ${}^3\text{He}({}^3\text{He}, 2p){}^4\text{He}$ reaction that operates at the base of the receding envelope of low-mass RGB stars produces locally an inversion of the mean molecular weight. Indeed, this reaction produces more particles than initially present. This μ -inversion generates hydrodynamical instabilities named thermohaline mixing and also referred to as salt finger instability. Based on this idea, Charbonnel & Zahn (2007) showed that stellar models accounting for this type of extra-mixing can explain the abrupt modification of the chemical abundances at the *bump*, thus reconciling theory and observation.

The similarities in the behaviors of observed abundances between field and globular clusters stars is however limited to Li, C and N. Indeed, although abundances of iron and heavy elements are relatively uniform within stars of a globular cluster², strong abundance variations of light nuclei are observed from star to star. Contrary to field stars, giants in globular clusters are characterized by a series of correlations/anti-correlations implying oxygen, sodium, magnesium and aluminium. In particular *systematic anti-correlations* between carbon and nitrogen, oxygen and sodium (Snedden 1999; Ramírez & Cohen 2002) and more occasionally between magnesium and aluminium (Gratton et al. 2001; Sneden et al. 2004) are

² ω Cen represents a notable exception by many other aspects (total mass, spatial distribution of stars and chemical composition).

observed. Let us note that in this latter case, the interpretation is not easy because of the difficulty to determine the exact magnesium isotopic composition. A rich literature discusses these chemical anomalies and we refer the reader to the reviews by Ivans et al. (2001), Ramírez & Cohen (2002) or Decressin (2007) and to the contribution of Corinne Charbonnel in this volume for further information.

With the advent of 8 meters telescopes, it was finally possible to probe the base of the RGB and the *turn-off*³ in various globular clusters (Gratton et al. 2001; Thévenin et al. 2001; Briley et al. 2004b). These observations reveal that the carbon/nitrogen (Briley et al. 2004a; Da Costa et al. 2004) and sodium/oxygen (Carretta et al. 2004) anti-correlations are already present on the main sequence. This result unambiguously attests of their primordial origin and of the necessity to account for a previous stellar population which contaminated the matter from which the stars of the cluster we observe now were formed.

1.5 Helium burning

1.5.1 He ignition

In low-mass stars ($M \lesssim 2 - 2.5M_{\odot}$), electron degeneracy becomes important (at the center the degeneracy parameter $\eta \simeq 2 - 3$). This causes a drop in the opacity (due to heat conduction) and allows the core to radiate away its energy more readily. At the same time, the maximum temperature moves off-center as plasma-neutrinos⁴ carry away some of the internal energy from the densest (central) part of the star. In these degenerate conditions, the pressure is weakly dependent on

³The *turn-off* corresponds to the location in the HR diagram where the evolutionary track turns back to cooler effective temperatures. This point marks the end of core H-burning.

⁴In dense environments at temperature $T > 10^8$ K, electrons interact with other electrons to emit neutrinos and anti-neutrinos, instead of photons.

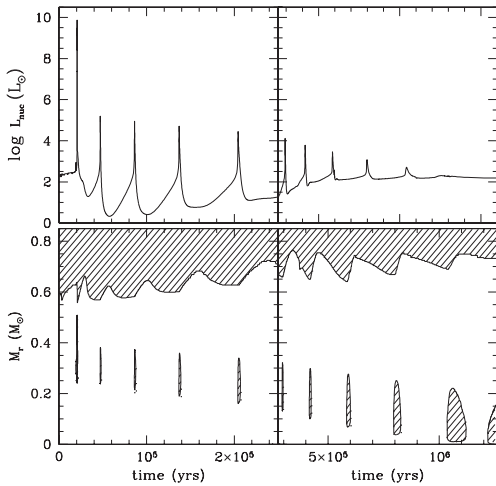


Fig. 4. Helium flash in a population III ($Z = 0$) star of $1 M_{\odot}$. The upper panel shows the evolution of the nuclear luminosity and the bottom panel the internal structure. Hatched areas represent convective regions (from Siess et al. 2002).

the temperature and the thermal and mechanical structures are almost decoupled. When He burning is initiated (above $T_{\max} \simeq 10^8\text{K}$), the increase in temperature is not followed by an expansion of the structure which would produce a cooling. On the contrary, the layers heat up, which contributes to further increase the nuclear energy production ($\varepsilon_{\text{nuc}}(3\alpha) \propto T^{40}$) and the system runs away. During this *thermonuclear helium shell flash*, a strong temperature gradient develops and a convective zone forms. The released energy⁵ is used to lift the core degeneracy and to expand the structure. The dilatation extinguishes the HBS and eventually the instability shuts down. At the end of the He-flash, the peak temperature has moved inward by $\sim 0.03 M_{\odot}$ (Mengel & Sweigart 1981; Siess et al. 2002) and the convective envelope has slightly withdrawn (Fig. 4). Thereafter a series of secondary flashes gradually lift the core degeneracy and allow the maximum temperature to reach the center. The first flash is by far the strongest one because of the higher core degeneracy at this time. As the flashes become weaker, their mass extent decreases and the time interval between successive instabilities also increases (Despain 1981).

The hydrodynamic nature of the helium flash is still a matter of debate (e.g. Deupree 1996) and the mixing processes associated with the development of the convective instability deserve additional studies. It is worth noticing that before He burning reaches the center, shells made essentially of carbon and oxygen (produced in the previous He flashes) surround the He-rich core. In these circumstances, the mean molecular weight gradient decreases in the direction of gravity and the layers become secularly unstable. These conditions are characteristics of the so-called thermohaline convection or *salt finger* instability seen before at the *bump*.

In stars more massive than $2 - 2.5 M_{\odot}$, the core temperature is higher, and so degeneracy and neutrino energy losses are much weaker. The maximum temperature thus remains at the center and helium ignites “quietly” under non-degenerate conditions. Thereafter, in both low- and intermediate-mass stars, He burning proceeds in a convective core.

1.5.2 Nucleosynthesis

When the central helium abundance drops below $Y \lesssim 0.1$, the $^{12}\text{C}(\alpha, \gamma)^{16}\text{O}$ reaction becomes faster than the 3α reactions and carbon starts to be destroyed to the benefit of oxygen. At the end of He burning, the mass fraction of carbon in the center (which depends on the metallicity and stellar mass) ranges between 0.1 - 0.4, the remainder consisting mainly of oxygen (Straniero et al. 2003). The central C/O ratio depends sensitively on the still highly uncertain $^{12}\text{C}(\alpha, \gamma)^{16}\text{O}$ rate and also on the treatment of convection which influences both the burning lifetime and the amount of fuel available (Imbriani et al. 2001). From a nucleosynthetic point of view, besides converting ^4He into ^{12}C and ^{16}O , core helium burning contributes to the destruction of the by-products of the H burning. Successive α -captures will transform ^{14}N into ^{18}O and ^{22}Ne . At sufficiently high temperatures ($T \gtrsim 3 \times 10^8\text{K}$)

⁵The nuclear luminosity associated with He burning can reach $10^{11} L_{\odot}$.

which are only found in massive stars ($M \gtrsim 15 M_{\odot}$), the $^{22}\text{Ne}(\alpha, n)^{25}\text{Mg}$ reaction releases a very great deal of neutrons which will participate to the production of heavy elements through the so called s-process (see §2.3.3). In convective regions such as the He-core of massive stars or the thermal pulses in AGB stars, efficient mixing keeps bringing the abundant iron seed nuclei at the base of the convective zone where the neutrons are released. As a result iron group nuclei capture most of the neutrons to the detriment of heavier elements. The weak irradiation of heavy elements generally prevents the nucleosynthesis of atoms beyond $A \sim 90$.

2 The AGB phase

Near the end of central He burning, the core starts to contract to compensate for the decrease in nuclear energy production. As for the 1DUP, the surface layers expand and the convective envelope deepens. With the exhaustion of fuel, convection disappears at the center and He burning proceeds in a shell surrounding the newly formed CO core. The activation of shell burning releases enough energy to temporarily halt and reverse the inward advance of the convective envelope (Fig. 1). In more massive stars, the expansion produces the quenching of the hydrogen-burning shell (HBS). The extinction of H burning then allows the penetration of the convective envelope through the formally active HBS down to the upper layers of the HeBS. Note that in massive stars the 2DUP does not have the ability to decrease the mass of the H-depleted core. The star thus develops a massive core (larger than the Chandrasekhar mass) that inevitably collapses. Similarly to the first dredge-up, the products of H burning (^4He , ^{14}N et ^{13}C mainly) are brought to the surface and for the most massive stars, He enhancement can also be substantial.

During the subsequent *early-AGB phase*, the core contracts and becomes more degenerate as the neutrino loss rate increases. The burning shells narrow and get closer to each other while the nuclear energy production is progressively transferred from the HeBS to the HBS.

2.1 Structure and evolution of AGB stars

The AGB (Asymptotic Giant Branch) phase represents the ultimate nuclearly active evolutionary stage of low- and intermediate-mass ($M \lesssim 9 M_{\odot}$)⁶. It ends with the ejection of the envelope during the “super-wind” phase (Vassiliadis & Wood 1993) that leads to the formation of a planetary nebula. During the post-AGB evolution, the newly formed white dwarf radiates away its internal energy and becomes cooler and more degenerate.

The structure of an AGB star is composed of a degenerated and inert core of $0.5 \lesssim M_{\text{WD}}/M_{\odot} \lesssim 1$, essentially made of carbon and oxygen. The precise C/O ratio depends on He burning conditions and typically ranges between 0.10 – 0.40.

⁶Binary stars are of course excluded from this statement.

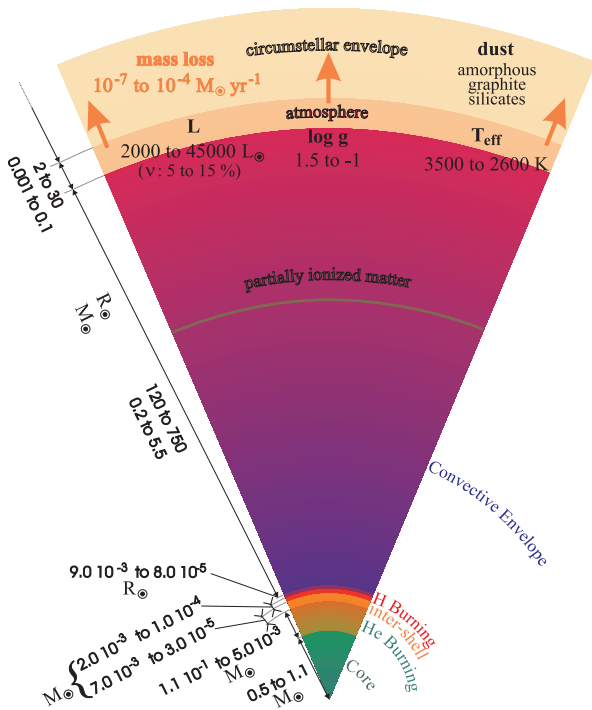


Fig. 5. Structure of an AGB star. The scales are indicated in the figure (borrowed from Manuel Forestini).

This compact core (of $< 10^5$ km in diameter) is surrounded by a thin helium-burning shell ($0.005 \lesssim M_{\text{HeBS}}/M_{\odot} \lesssim 0.1$) which is the siege of recurring instabilities: the thermal pulses. This layer is surmounted by a radiative zone, the *intershell*, made of the ashes of H burning and too cold for He burning. Above the *intershell*, hydrogen is burnt in a thin layer of $3 \times 10^{-5} \lesssim M_{\text{HBS}}/M_{\odot} \lesssim 2 \times 10^{-3}$. Note that a thin radiative layer is generally present that separates the HBS from the convective envelope. In case of *Hot Bottom Burning*, this buffer layer disappears and the surface luminosity is strongly modified (see 2.3.2). Finally a large convective envelope representing more than 99% of the radius surrounds this nuclearly active core. The envelope suffers important mass loss whose rate increases along the asymptotic branch to reach values as high as $10^{-4} M_{\odot} \text{ yr}^{-1}$ during the final super-wind phase. The surface layers of this extended convective zone are also subject to hydrodynamical instabilities that make them pulsate (MIRA variables). Outside the star, at larger distances, dust and grains form in an extended circumstellar envelope.

AGB stars represent a unique site for nucleosynthesis where the products of hydrogen burning are injected into the high temperature region of helium burning. This particular alchemy takes place during the thermal pulses that I describe in the following section.

2.1.1 The thermal pulses

AGB stars are characterized by the development of recurrent instabilities in the helium-burning shell. Schwarzschild & Härm (1965) were the first ones to discover and theoretically explain this phenomenon. They showed that 3 conditions are necessary for a burning shell to become unstable: the layer must be geometrically thin, the thermonuclear reaction rates must exhibit a strong temperature dependence and, finally, the opacity of the matter must be high. To understand this mechanism, imagine that some nuclear energy (e.g. associated with the ignition of the 3α reactions) is suddenly released in a small region of the star, thin in radius (the He burning shell). The temperature increase associated with this energy deposition naturally induces the expansion of the burning layer but, given its thinness this swelling does not cause a noticeable displacement of the layers surrounding it. The mechanical structure of star thus remains practically unchanged, except obviously in an extremely localized area where the *relative* variation of the shell thickness is very large. Hydrostatic equilibrium is barely disturbed by these negligible changes in radius and the region of energy production becomes unstable because the temperature increase is not compensated by a rise in pressure. Furthermore, if in this shell the opacity is high and the nuclear reaction rates are strongly dependent on temperature, the energy cannot be evacuated efficiently and accumulates. In AGB stars, these conditions are met in the HeBS and give rise to the development of the thermal pulses.

The evolution of the star during the AGB phase is characterized by the alternate activation of H and He shell burning (Fig. 6). During the thermal pulses (which last at most a few hundred years), energy is almost entirely provided by He burning, whereas during the interpulse (which can last several tens of thousands of years), hydrogen burning, ensures more than 90% of the energy demand (mainly through the CNO cycle). Because of this alternate burning mode, the helium and hydrogen layers separate and the intershell grows in mass during the interpulse. The pressure and temperature in the HeBS increase due to core contraction and the 3α reactions eventually re-ignites. The temperature gradient changes abruptly and a convection zone appears: the thermal pulse. This instability grows quickly and engulfs the region previously occupied by the HBS. As a piston, the thermal pulse pushes the layers of the star to larger (and cooler) radii, which produces the lifting of the base of the envelope and the quenching of the HBS. Deprived of an important energy source, the star contracts (Fig. 6). In a few hundred years, the pulse reaches its maximum extension. The radiative zone separating the nuclear region from the envelope is now thin enough so that the excess of energy released by the instability can efficiently flow to the nearby envelope where it is evacuated to the surface by convection. After ~ 180 yr in our example, the instability dies out and the bottom of the convective envelope moves inward, releasing the potential energy stored during the pulse.

During a thermal pulse $10^5 L_{\odot}$ to $\sim 10^9 L_{\odot}$ can be released, the value depending on the metallicity, stellar mass and evolutionary status of the star. In general, the strength of the instability, as measured by the nuclear luminosity associated

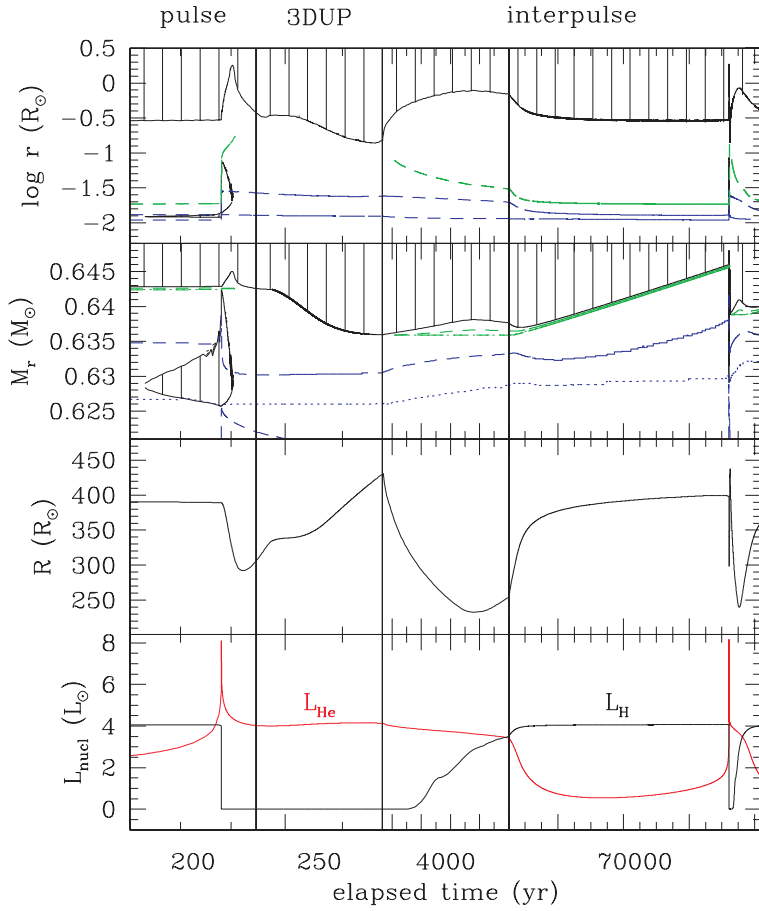


Fig. 6. Evolution during a pulse-interpulse cycle of the nuclear luminosities associated with hydrogen (L_{H}) and helium (L_{He} , lower panel) burning, of the radius (R) and of the internal structure of the star in Lagrangian (M_r) and eulerian coordinates (top). The model is a $3M_\odot$ of solar metallicity in which mixing due to overshooting (with $f_{\text{over}} = 0.016$ as defined by Eq. 2.2) was included. The convective zones are hatched and the dashed lines delineate the regions of nuclear energy production associated with helium and hydrogen burning, respectively. A third *dredge-up* episode is present after the extinction of pulse. The duration of each phase (pulse-3DUP-interpulse) is indicated in the x-coordinate.

with He burning (L_{He}), increases with core mass and with decreasing metallicity. The duration of the pulses varies slightly according to the stellar parameters and typically amounts to a few hundred years. The mass of the pulse is small, between 10^{-4} and $10^{-2} M_\odot$, and the maximum temperature at its base can reach $3.5 \times 10^8 \text{K}$.

2.1.2 The third *dredge-up*

With the decay of the thermal pulse, the convective envelope moves back to its initial position and in some cases⁷ it penetrates into the layers that were previously occupied by the pulse. During the so-called third *dredge-up* (3DUP thereafter), the products of the pulse nucleosynthesis are brought to the surface by the convective motions. The 3DUP is not a phenomenon easy to initiate in stars for different reasons : the envelope, mainly made up of hydrogen and of helium must cross an important barrier of molecular weight to penetrate in the carbon and oxygen-rich layers of the pulse. Moreover, the 3DUP is a process which costs energy to the star because convection must provide additional work against gravity to lift the heavy elements of the pulse (C and O) into the envelope (made principally of H and He).

The literature on the modeling of the AGB stars reveals that the characteristics of the 3DUP (their time of first appearance and their depth for example) notably vary from one simulation to another and depend on many factors that include the algorithm for the definition of the convective boundaries (Lattanzio 1989; Frost & Lattanzio 1996), the choice of the mixing length parameter in the convective zone (Boothroyd & Sackmann 1988b), the assumptions concerning the treatment of the entropy of mixing (Wood 1981), the spatial and temporal resolutions (Straniero et al. 1997), numerical aspects related to the resolution of the stellar structure equations (Pols & Tout 2001; Stancliffe 2006) or the presence of mixing processes at the base of the convective envelope (Herwig et al. 1997; Mowlavi 1999; Siess et al. 2003). These works illustrate the difficulties of this modeling which remains essentially very sensitive to the treatment (numerical and/or physical) of the convective borders.

The presence of mixing at the base of the convective zone reveals very efficient – if not mandatory – to the establishment of the 3DUP (Mowlavi 1999). By considerably lowering the molecular weight gradients between the envelope and the core, the mixing processes strongly facilitate the penetration of convection in the inner regions. The physical origin of mixing is still unclear but transport mechanisms associated with overshooting, stellar rotation or gravity waves are the most popular. The description of the first two processes will be given in the next sections.

Strong pulses, characterized by a high helium luminosity, tend to favor the occurrence of the 3DUP. The explanation is due to the fact that when more energy is released, the luminosity of the intershell is higher, and according to the Schwarzschild criterion⁸, if L increases, $\nabla_{\text{rad}} (\propto L)$ also increases and can become

⁷This depends on metallicity, pulse strength, core mass, numeric, ... see §2.4.

⁸The Schwarzschild criterion states that a shell is convective if $\nabla_{\text{rad}} > \nabla_{\text{ad}}$ where ∇_{ad} is the adiabatic gradient and ∇_{rad} the radiative gradient whose expression is given by

$$\nabla_{\text{rad}} \equiv \left. \frac{d \ln T}{d \ln P} \right|_{\text{rad}} = \frac{3}{16\pi ac\mathcal{G}} \frac{\kappa L P}{M_r T^4} .$$

T, P, L, κ and M_r representing the temperature, pressure, luminosity, opacity and the mass

larger than ∇_{ad} , turning the shell convective. Another condition favorable for the deepening of the envelope is that the HBS be extinct to avoid any temperature inversions at the base of the envelope.

To characterize the 3DUP, the literature usually refers to the parameter λ defined as

$$\lambda = \frac{\Delta M_{\text{DUP}}}{\Delta M_{\text{H}}}, \quad (2.1)$$

where ΔM_{DUP} represents the mass dredged-up by the convective envelope (mass comprised between the top of pulse and the base of the envelope at its deepest extent during the 3DUP) and ΔM_{H} the core mass increase due to HBS during the preceding interpulse period. With this definition $\lambda = 0$ means absence of 3DUP and $\lambda = 1$ means absence of core mass increase. This parameter is fundamental because it determines the efficiency of envelope pollution by the products of the pulse nucleosynthesis, which in turn affects the yields. Recent calculations (Karakas et al. 2002) indicate that the value of this parameter saturates quickly after 5 – 10 pulses. These simulations also provide general trends, namely that for a given mass, λ increases when the metallicity decreases and, for a given metallicity, λ increases with the stellar mass (Wood 1981; Boothroyd & Sackmann 1988b). Moreover it appears that below a critical envelope mass ($M_{\text{crit}}^{\text{env}} \lesssim 0.2M_{\odot}$), the 3DUP ceases (Wood 1981; Straniero et al. 1997). The duration of the interpulse phase is a decreasing function of the core mass (e.g. Boothroyd & Sackmann 1988a; Wagenhuber & Groenewegen 1998) and varies typically between 500 and 10^5 yr. From a practical point of view, the modeling of the interpulse phase represents more than 90% of the computing time of a full pulse-interpulse cycle.

At the end of the 3DUP, the HeBS is extinguished and when the HBS re-ignites the envelope retreats. The star enters the interpulse phase, during which the mass of the intershell grows by the accumulation of the nuclear ashes coming from the HBS. The envelope follows the advance of the HBS and, in the HR diagram, the star climbs the Asymptotic Giant Branch as its radius and luminosity increase.

2.2 Rotating AGB stars

Rotation affects stellar structure in two ways. First it generates centrifugal forces which alter the mechanical and thermal balance of the star and on the other hand it is a source of mixing which modifies the stellar chemical composition. The centrifugal forces contribute to support the structure by decreasing the effective gravity but as far as AGB stars are concerned, their effects on the evolution are weak (Siess et al. 2003). Rotating AGB stars have a slightly cooler HBS leading to longer interpulse periods and since the core mass at the next pulse is larger, the strength of the He shell flash is also slightly increased.

But the main effect comes from the incorporation of rotational mixing which is able to trigger the 3DUP contrarily to the non-rotating model where it is absent.

contained inside radius r , respectively.

By favoring the development of 3DUP episodes, rotation significantly modifies the envelope chemical composition, the mass loss rate and thus, its subsequent evolution. Rotational mixing proceeds as follows : at the end of central He burning, angular momentum is stored in the contracting core. Later, during the AGB phase, the thermal pulses are able to reach this reservoir and allow the extraction and redistribution of angular momentum (AM) in the intershell region (Fig. 7). When the instability deactivates, a fast rotating zone is left in place of the pulse which is subject to rapid structural readjustments. In the contracting layers, the rotational velocity increases and where expansion occurs, it slows down. On a timescale of a few years, which does not allow for AM transport (Fig. 7), shear develops below the envelope and generates the turbulence that drives the mixing. By eroding the chemical composition discontinuity, rotational mixing allows the deepening of the envelope and the development of efficient 3DUP. It is important to note that shear is maximum at the base of the convective envelope because the slowly rotating envelope⁹ penetrates in the accelerated region of the pulse. During the subsequent interpulse phase, the transport of angular momentum lowers the gradients of angular velocity but a shear layer persists in a thin shell of $\lesssim 10^{-4} M_{\odot}$ at the location where the convective envelope reached its deepest extent, precisely where the s-process is expected to take place.

The evolution during the 13 first pulses of a $3 M_{\odot}$, $Z = Z_{\odot}$ star is shown in Fig. 7. At first sight, we note that the spatial extension of the mixing zone (colored area) strongly decreases during the course of the evolution. At the beginning of the AGB phase, rotational mixing extends over the area located between the core and the envelope whereas during later pulses, it is confined to a more restricted fraction of this zone. This decreasing efficiency of rotational mixing is mainly a consequence of core growth (Siess et al. 2003). Indeed, as the mass of the future white dwarf increases, the base of the pulse moves away from the central angular momentum reservoir. By dredging up smaller amounts of momentum, the pulse generates a weaker differential rotation and thus less mixing. This explains the reduction in strength and duration of the transport process along the AGB phase.

In conclusion, in AGB stars the mechanical effects of rotation are secondary in comparison with the modifications induced by rotational mixing.

2.3 Nucleosynthesis

A particularly complex and rich nuclear activity is taking place in the thermal pulses. The occurrence of 3DUP episodes allows the products of this nucleosynthesis to reach the stellar surface where they are observed. In this section, the nucleosynthesis of the pulse, envelope and that of the s-process will be reviewed successively.

⁹The envelope rotation rate is slow because its momentum of inertia is much larger than that of the core.

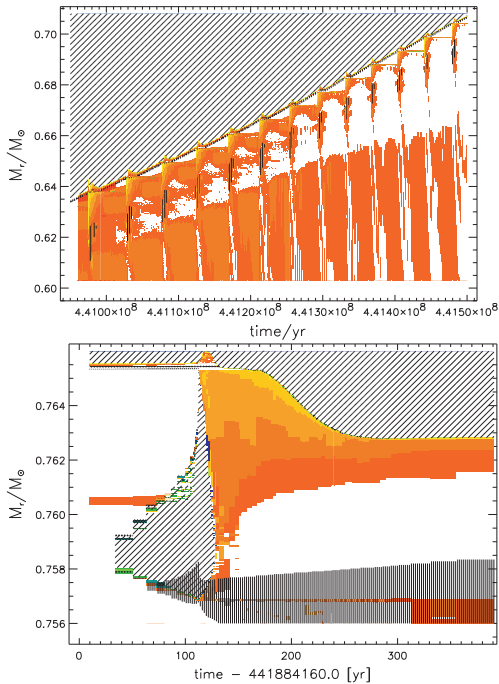


Fig. 7. Evolution of the internal structure of a rotating $3 M_{\odot}$ AGB star of $Z = Z_{\odot}$. The range of colors indicates the amplitude of the coefficient of diffusion. Lighter colors indicate larger differential rotation and thus more efficient mixing. The upper figure shows the evolution during the 13 first pulses. On this figure the thermal pulses cannot be resolved but their occurrence can be traced from the lifting of the convective envelope and by the increasing mixing (light colored zones). The lower panel concentrates on the 29th pulse and subsequent 3DUP (From Siess et al. 2003, 2004). Mixing is essentially concentrated at the base of the convective envelope represented by the upper shaded area.

2.3.1 Pulse nucleosynthesis

Helium burning provides the energetics of the pulse and leads to the production of ^{12}C and of ^{16}O by way of the 3α and $^{12}\text{C}(\alpha, \gamma)$ reactions, respectively. The ashes of H burning (as a result of CNO cycling mainly) are made up of ^{14}N , ^{13}C and ^{15}N , and are ingested in the convective pulse. The remaining¹⁰ ^{13}C is quickly burnt by $^{13}\text{C}(\alpha, n)^{16}\text{O}$, releasing neutrons which are absorbed by the abundant ^{14}N and by the iron peak elements. ^{14}N is mainly destroyed by α -capture reactions $^{14}\text{N}(\alpha, \gamma)^{18}\text{O}$ and $^{14}\text{N}(\alpha, \gamma)^{22}\text{Ne}$ which lead to the production of ^{18}O and ^{22}Ne . The other main nitrogen isotope, ^{15}N is principally destroyed by $^{15}\text{N}(\alpha, \gamma)^{19}\text{F}$. At higher temperatures ($T > 2.8 \times 10^8 \text{K}$), fluorine is destroyed by $^{19}\text{F}(\alpha, p)^{22}\text{Ne}$. Finally, if the temperature at the base of the pulse reaches $3.2 \times 10^8 \text{K}$, the reactions $^{22}\text{Ne}(\alpha, n)^{25}\text{Mg}$ and $^{22}\text{Ne}(\alpha, \gamma)^{26}\text{Mg}$ are activated, leading to the production of the magnesium isotopes and to the release of a large number of neutrons that will participate to the convective s-process.

2.3.2 Hot Bottom Burning

In massive and/or low metallicity AGB stars, the temperature at the bottom of the convective envelope (T_{env}) is sufficiently high that hydrogen burning is activated

¹⁰Most of the ^{13}C burns radiatively in the intershell during the interpulse phase, see §2.3.4.

at its base : this phenomenon is called *Hot Bottom Burning* (HBB thereafter). When $T_{\text{env}} \gtrsim 3 \times 10^7 \text{K}$, HBB enables the production of ${}^7\text{Li}$ by the Cameron & Fowler (1971) mechanism. In this process, ${}^7\text{Be}$ is produced at the base of the envelope by the pp cycle (more precisely by ${}^3\text{He}(\alpha, \gamma){}^7\text{Be}$) and transported by convection in the cooler external shells of the star before it is destroyed by electron captures to form ${}^7\text{Li}$. By coupling the evolution of the nuclear species (the nucleosynthesis equations) with the diffusion equations, a ${}^7\text{Li}$ profile establishes in the envelope. For some time the star appears as a lithium rich giant. However, when the reservoir of ${}^3\text{He}$ is exhausted the production of ${}^7\text{Li}$ stops and it is subsequently destroyed by proton-capture reactions. So, although the production of lithium can be important in AGB stars, this Li-rich¹¹ phase remains transitory and generally of short duration. The contribution of AGB stars to the galactic ${}^7\text{Li}$ production is very dependent on the mass loss rate during this phase but anyhow it remains negligible (see Travaglio et al. 2001, for a fuller discussion).

When the temperature at the base of the envelope reaches $T_{\text{env}} \gtrsim 5 \times 10^7 \text{K}$, the operation of the CNO cycle converts ${}^{12}\text{C}$ into ${}^{13}\text{C}$ and ${}^{14}\text{N}$ mainly. This results in a significant reduction of ${}^{12}\text{C}/{}^{16}\text{O}$ and ${}^{12}\text{C}/{}^{13}\text{C}$ ratios. But HBB does more than just burn ${}^{12}\text{C}$: it also allows the NeNa and MgAl chains to come into play. The activation of these H-burning reactions requires higher temperatures ($T_{\text{env}} \gtrsim 6 \times 10^7 \text{K}$) which are met in the most massive and most metal-poor AGB stars. Proton-captures on the products of the pulse nucleosynthesis (${}^{22}\text{Ne}$, ${}^{25,26}\text{Mg}$) contribute to the production of ${}^{23}\text{Na}$, ${}^{26}\text{Al}$ and ${}^{27}\text{Al}$. Finally, HBB destroys efficiently ${}^{19}\text{F}$ by ${}^{19}\text{F}(\text{p}, \alpha){}^{16}\text{O}$ which closes the CNOF cycle.

At solar metallicity, HBB develops in stars more massive than $M \geq 4 - 5 M_{\odot}$ but in primordial stars, this limit is lowered to $M \simeq 2 M_{\odot}$ (Siess et al. 2002). Finally, let us note that in some stars (primordial massive AGB stars or super-AGB stars), the temperature at the base of the envelope exceeds 10^8K . Under these conditions, ${}^{23}\text{Na}$ and ${}^{24}\text{Mg}$ are burnt to the benefit of the heavier Mg and Al isotopes. A summary of this rich nucleosynthesis is presented in Fig. 8.

2.3.3 Introducing the s-process

S-elements are heavy atoms located on the valley of stability beyond the iron peak elements in the periodic chart of nuclei. Their nucleosynthesis results from the succession of slow neutron captures (*s* for *slow*) followed by β^+ -decays, starting from the iron peak elements and up to bismuth 209 (Fig. 9). Beyond ${}^{209}\text{Bi}$, the following chain of reactions ${}^{209}\text{Bi}(\text{n}, \gamma){}^{210}\text{Bi}(\beta^+){}^{210}\text{Po}(\gamma, \alpha){}^{206}\text{Pb}$ closes the cycles and puts an end to the s-process. Heavier elements such as uranium require more intense neutron flows and are synthesized by the *r*-process (*r* for *rapid*, see Marcel Arnould in this volume). The most popular, and well-known as the classical s-process model, is based on the original canonical model of Burbidge et al. (1957) and was first successfully developed by Clayton et al. (1961). The canonical model assumes that some stellar material composed of iron nuclei only is subject to a

¹¹In some stars, the lithium abundance $\epsilon({}^7\text{Li}) = \log \frac{\text{Li}}{\text{H}} + 12 > 5$.

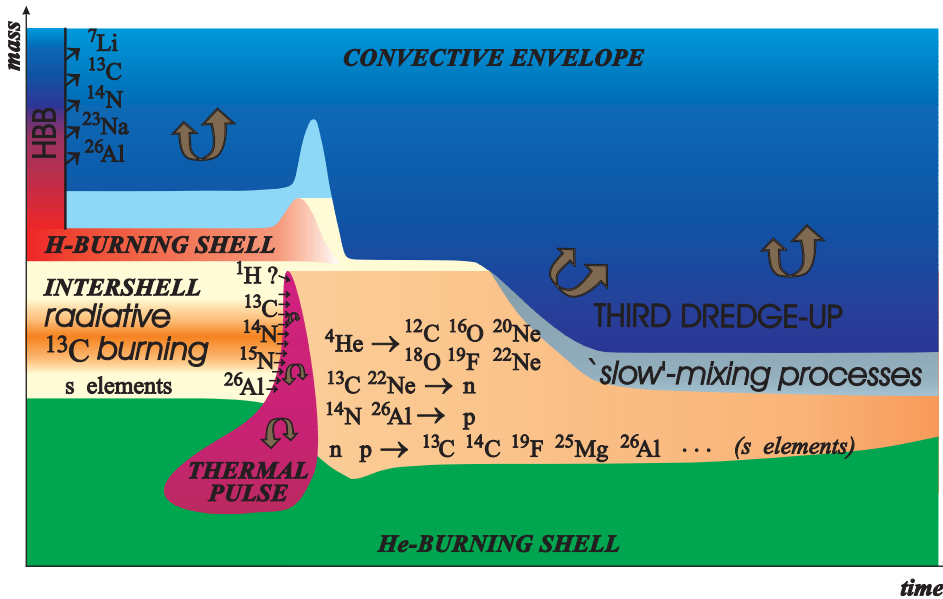


Fig. 8. Summary of the various nucleosynthesis sites and chemical species implied during AGB evolution (figure designed by M. Forestini).

constant neutron irradiation characterized by the fact that the neutron density is low enough for the β -decays of unstable nuclei to be faster than the neutron captures. Rapidly, it turned out that the solar system s-abundances could not be explained as originating from a single neutron exposure¹². The solar s-element composition was therefore assumed to be the result of a superposition of different distributions of neutron exposures. The solar s-abundance distribution clearly indicates that the stronger the neutron irradiation, the less probable it becomes. In particular, Clayton et al. (1961) showed that an exponential or power-law neutron exposure distribution could efficiently do the work. This model has been very successful in reproducing the solar system s-abundance distribution by considering the superposition of three exponential distributions: the weak component essentially responsible for the production of the $70 \leq A \leq 90$ s-nuclei, the main component for the $90 \leq A \leq 204$ isotopes and the strong component for the Pb and Bi elements (e.g. Kappeler et al. 1989).

¹²The neutron exposure is given by $\tau = \int N_n(t') v_T dt'$, where N_n is the neutron density, v_T the thermal velocity of neutrons. It is measured in mbar^{-1} . At solar metallicity, a typical s-process nucleosynthesis occurring in an intermediate-mass AGB star is characterised by $\tau \sim 0.6 - 1 \text{ mbar}^{-1}$.

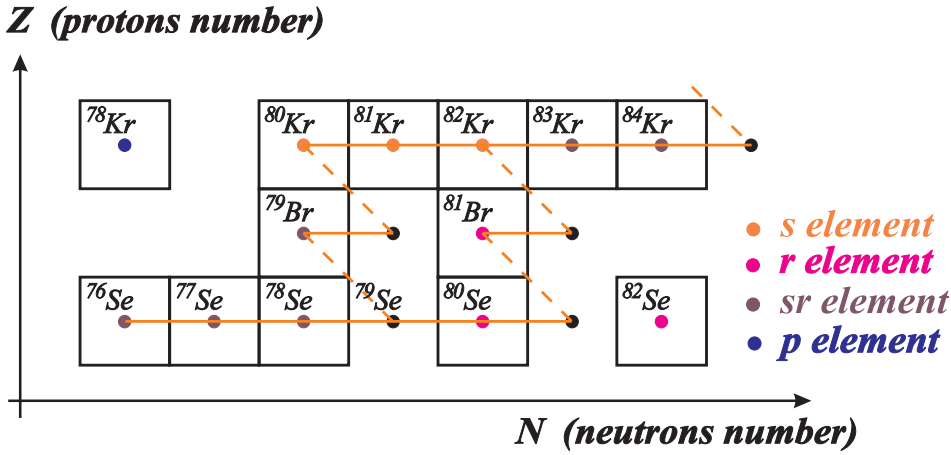


Fig. 9. Schematic s-process path. ^{79}Se represents a branching point in the s-process path. If the neutron flux is low, the formation of ^{79}Br and $^{80,81}\text{Kr}$ is favored. On the other hand, for larger neutron fluxes, the path will take the other branch and the synthesis of ^{80}Se , ^{81}Br will be favored. Neutron-rich elements that cannot be made by the s-process, such as ^{82}Se , are referred to as r-elements and proton-rich species, such as ^{78}Kr , as p-elements (see Marcel Arnould in this volume for details on these nucleosynthetic processes).

2.3.4 The s-process in AGB stars

The production of the *heavy s-elements* (mass number $A \gtrsim 90$) is ensured by two main neutron sources : the $^{22}\text{Ne}(\alpha, n)^{25}\text{Mg}$ and $^{13}\text{C}(\alpha, n)^{16}\text{O}$ reactions. The first one requires relatively high temperatures ($T \gtrsim 3 \times 10^8 \text{K}$) which can only be found at the base of hot pulses, i.e. in massive and/or low metallicity stars (typically for $M \gtrsim 3 M_{\odot}$). From an observational point of view, this neutron source is not the most privileged one because it should produce a strong correlation between the overabundances of ^{25}Mg and s-elements, which is not observed (e.g. Smith & Lambert 1986a; McWilliam & Lambert 1988). Note however that the constraints on ^{25}Mg mainly come from observations of low-mass AGB stars which, in any case, cannot activate the $^{22}\text{Ne}(\alpha, n)$ neutron source. Besides, s-elements are present in stars of low-luminosity, i.e., in low-mass AGB stars ($M \lesssim 2.0 M_{\odot}$) where the temperature at the base of the pulse is certainly lower than the $3.2 \times 10^8 \text{K}$ required for the activation of this reaction (Frogel et al. 1990). Finally if this neutron source was efficiently working in AGB stars, it would affect the branching points at ^{85}Kr , ^{87}Rb and ^{95}Zr , which is not confirmed observationally (Lugaro et al. 2003).

The second source, associated with $^{13}\text{C}(\alpha, n)^{16}\text{O}$, is activated at lower temperatures ($T \gtrsim 9 \times 10^7 \text{K}$) and has the favour of the theoreticians. However the formation of a substantial amount of ^{13}C (the famous *^{13}C pocket*) necessary for the neutron production remains a major theoretical problem. Indeed, the mass of ^{13}C contained in the HBS and injected into the pulse is insufficient to account for

the production of s-elements. Iben & Renzini (1982) were the first to suggest that ^{13}C nuclei could be produced at the time of the 3DUP by the diffusion of protons from the envelope in the underlying radiative layers enriched in carbon by the passage by the pulse. In this context, ^{13}C is synthesized by $^{12}\text{C}(p,\gamma)^{13}\text{N}(\beta^+)^{13}\text{C}$ and its subsequent radiative burning during the interpulse leads to the synthesis of s-elements (Fig. 10). However, the mechanism at the origin of proton mixing at the time of the 3DUP is not clearly identified: the various scenarios call upon overshooting (Herwig et al. 1999; Goriely & Mowlavi 2000), rotation (Langer et al. 1999; Herwig et al. 2003; Siess et al. 2004) or gravity waves (Denissenkov & Tout 2003). Parametric models, assuming an arbitrary ^{13}C profile in the intershell (Gallino et al. 1998; Busso et al. 2001) can account for the observed distributions of s-elements provided the mass of the pocket varies by more than three orders of magnitude. Although these studies do not provide any insight on the physical process responsible for the formation of the ^{13}C pocket, they give information on the required ^{13}C mass necessary to reproduce the observations. As pointed out by Lugaro et al. (2003), the abundance of ^{13}C formed after proton injection depends linearly on the intershell carbon mass fraction which has been built up during the previous thermal pulse. Since the carbon abundance depends on the amount of extra-mixing present at the base of the He shell flash it turns out that the details of the s-process depend on the type of mixing operating not only at the base of the envelope but also at the bottom of the convective pulse !

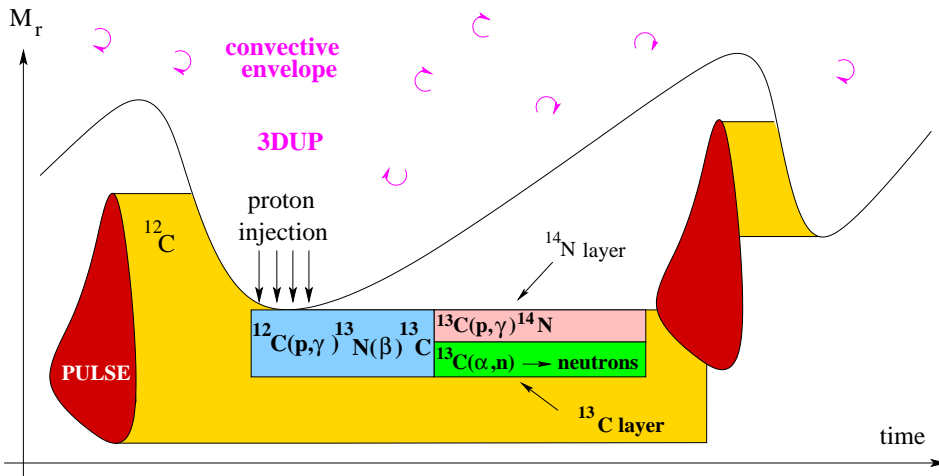


Fig. 10. The injection of protons at the base of the envelope during the 3DUP by some unidentified mixing process leads to the formation of a ^{14}N -rich layer just below the envelope that surmounts the ^{13}C pocket. This latter element is subsequently burnt radiatively during the interpulse and the released neutrons participate to the s-process nucleosynthesis. The s-elements are then engulfed in the pulse and brought to the surface of the star during the subsequent 3DUP.

Overshooting In the framework of the mixing length theory (MLT), the determination of the convective borders is based on local considerations – the Schwarzschild or the Ledoux criterion – and does not account for the inertia of the globules. In the MLT, the fluid elements have a non-zero velocity at the radiative boundary and their deceleration beyond the formal convective border represents an additional source of mixing referred to as *overshooting*. Hydrodynamic simulations of convection in A-type stars (Freytag et al. 1996) showed that mixing at the base of the convective envelope (of a main sequence star) could be treated by a diffusive process with an exponentially decreasing diffusion coefficient. The general expression is given by

$$D_{\text{over}}(r < r^{\text{env,bot}}) = D_{\text{conv}}^{\text{env,bot}} \times e^{-\frac{(r^{\text{env,bot}} - r)}{f_{\text{over}} \times H_{\text{p}}^{\text{env,bot}}}} \quad (2.2)$$

where $r^{\text{env,bot}}$ and $H_{\text{p}}^{\text{env,bot}}$ are the radius and pressure scale height at the bottom of the convective envelope and f_{over} is a free parameter characterizing the extent of the partial mixing zone. This simple and easy implementable parametrization of overshooting has motivated new studies mainly in the context of AGB stars (Herwig et al. 1997, 1999).

The impact of overshooting on the s-process nucleosynthesis has been analyzed in detail by Goriely & Mowlavi (2000). The authors have shown that the production of ^{13}C depends on the proton-to-carbon ratio ($X_{\text{p}}/X_{12\text{C}}$, where X represents the mass fraction of the element) in the partial mixing (PM) zone. In the top part of the mixed region where the proton abundance is high ($X_{\text{p}}/X_{12\text{C}} \gtrsim 10^{-2}$), the CN-cycle reaches equilibrium and leads to a large production of ^{14}N . Below this nitrogen-rich layer, where $10^{-3} \lesssim X_{\text{p}}/X_{12\text{C}} \lesssim 10^{-2}$, ^{13}C is mainly produced. Finally, deeper in the star the scarcity of the protons avoids significant modification of the abundances. Schematically the proton mixing zone consists of a ^{14}N layer sitting on top of the ^{13}C pocket where the neutrons are released (Fig. 10). In the partial mixing model, the s-process abundance distribution appears to be essentially a function of the stellar metallicity, as shown in Fig. 11. But the surface enrichment depends on the depth of the 3DUP, on the extent of the thermal pulse and on the envelope mass, and thus varies with stellar mass. In this scenario, all AGB stars, irrespective of their mass and metallicity, synthesize nuclei with $90 \lesssim A \lesssim 140$ in an almost solar distribution. In contrast, only low-metallicity stars ($Z \lesssim 0.001$) are expected to produce the heavier s-elements ($140 \lesssim A \lesssim 204$) efficiently.

The production of s-elements was also studied in primordial stars where the initial abundances are given by the Big Bang nucleosynthesis (Goriely & Siess 2001; Siess & Goriely 2002, 2003). In the absence of iron seeds, the neutrons are initially absorbed by the CNO and neon atoms that were synthesized by the star¹³. After the bottleneck associated with the reaction $^{33}\text{S}(n,\alpha)^{30}\text{Si}$ is passed, the neutron irradiation proceeds, producing elements of increasing mass number.

¹³These elements are said to be primary because their production depends only on the initial amounts of H and He which are almost independent of metallicity.

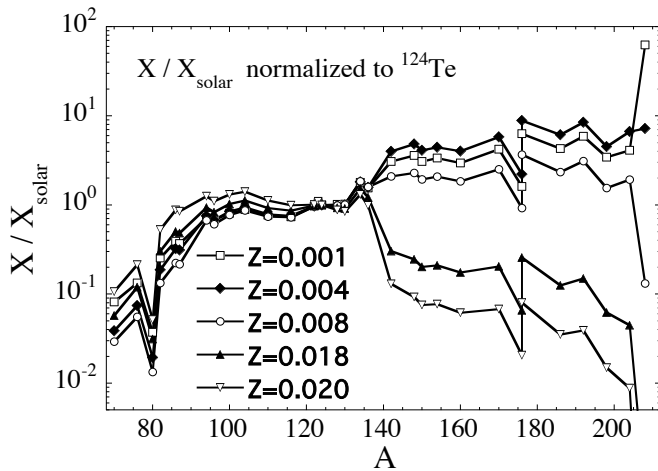


Fig. 11. Abundance distribution of s-only nuclei after partial proton mixing at the end of one interpulse phase as a function of metallicity. Abundances are normalized to the solar abundance of ^{124}Te (from Goriely & Mowlavi 2000).

With decreasing metallicity, the number of iron seed nuclei becomes smaller and in proportion more neutrons are made available for the other heavier elements synthesized during this process. The distribution of the s-nuclei is thus characterized by a large overabundance of ^{208}Pb and ^{209}Bi , a feature observed in very metal-poor giants (e.g. Van Eck et al. 2001).

The overshoot model cannot however account for the relatively modest abundances in lead and bismuth observed in some metal-poor stars (Aoki et al. 2000, 2002; Van Eck et al. 2003). Aoki et al. (2003) found that more than 70% of their sample of 33 carbon-rich metal-poor stars with $[\text{Fe}/\text{H}] < -2.5$ ¹⁴ have enhanced s-element abundances. These observations also indicate that, for a given metallicity, there is a strong dispersion of lead abundance, by more than 3 orders of magnitude, and that in more than 60% of the observed stars, these determinations are in disagreement with the theoretical predictions. This apparent incompatibility can however be circumvented if the diffusion of protons takes place during *hot* dredge-up where the temperature at the base of the envelope is high, i.e. when HBB operates efficiently. In this situation, the timescale for proton burning (~ 1 yr for $T_{\text{env}} \simeq 8 \times 10^7 \text{K}$) becomes comparable with the diffusion timescale and the coupling of the diffusion and nucleosynthesis equations is necessary. In these conditions, protons are burnt in fly as they diffuse below the envelope and the ^{13}C

¹⁴The standard notation means $[A/B] = \log \left[\frac{n(A)}{n(B)} \right]_* - \log \left[\frac{n(A)}{n(B)} \right]_{\odot}$, where $n(A)$ and $n(B)$

represent abundances per volume of species A and B in the star (*) compared to the solar value (\odot), respectively.

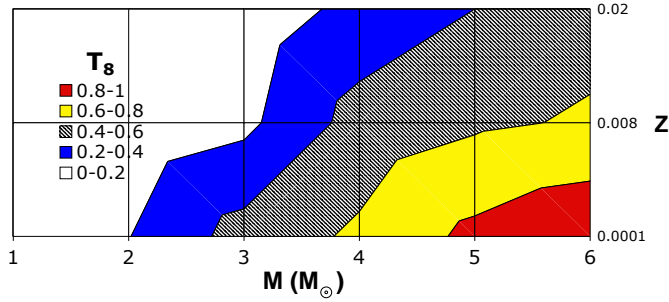


Fig. 12. Average temperature at the base of the convective envelope at the time of the 3DUP for a large set of AGB models with masses equal to $M = 1, 2, 3, 4, 5, 6 M_{\odot}$ and for metallicities $Z = 0.02, 0.008$ and 0.0001 . T_s represents the temperature in unit of $10^8 K$. In the high temperature region $T_s \gtrsim 0.7$ the s-process is not efficient because protons are burned during their transport and the ^{13}C and ^{14}N layers mix (from Goriely & Siess 2004).

and ^{14}N profiles that form during the process diffuse as well. Self-consistent simulations (Goriely & Siess 2004) indicate that the ^{13}C pocket ends up being entirely engulfed in the ^{14}N rich layer. The consequences are catastrophic for the s-process since the majority of the released neutrons are preferentially captured by ^{14}N instead of being absorbed by the heavy nuclei. The result is the quasi absence of s-elements production.

S-process nucleosynthesis in AGB stars thus reveals very sensitive to the thermodynamic conditions at the base of the convective envelope and to the (unknown) depth/efficiency of the mixing characterized by the overshoot parameter f_{over} . A systematic analysis of the average temperature at the base of the convective envelope at the time of the 3DUP provides a qualitative estimate of the metallicity and mass dependence of the efficiency of overshoot s-process in AGB stars (Fig. 12). In the low-temperature region ($T_{env} \lesssim 4 \times 10^7 K$), the s-process is particularly efficient while in hotter stars where $T_{env} \gtrsim 7 \times 10^7 K$ its action is very limited because protons are partially destroyed during their transport resulting in the mixing of the ^{13}C and ^{14}N layers. In the transition zone between these two regimes, the efficiency of the s-process is intermediate and could account for the observed spread in s-process abundances in low-metallicity AGB stars (Fig. 15). Figure 12 also shows that the efficiency of the s-process decreases as the stellar mass increases and the metallicity decreases.

Rotational mixing By nature, mixing associated with overshooting and gravity waves is directly connected to the spatial localization of the convective border. Within this framework, the formation of a pocket of ^{13}C results from the injection of protons into the carbon rich zone left by the pulse at the time of the 3DUP. Later on, when the envelope retreats, the chemical evolution of the layers affected by partial mixing only results from the action of the nuclear burning. When rotational

mixing operates, the situation is different because a relatively efficient mixing is maintained during the interpulse in the region where protons were initially injected (see §2.2).

At the time of the 3DUP, the strong differential rotation present at the base of the convective envelope leads to the injection of protons in the underlying carbon rich layers. After ~ 800 years, the ^{13}C pocket forms just below the ^{14}N rich shell, as in the overshooting model. However the persistence of shear in the partial mixing layer during the interpulse allows for the transport of nitrogen into the ^{13}C buffer where the s-process takes place. Subsequently ^{14}N absorbs a large fraction of neutrons, which inhibits the production of the s-elements. The resulting s-abundances are extremely low (Siess et al. 2003, 2004; Herwig et al. 2003) and this failure to synthesise heavy elements represent a major flaw to the rotational mixing scenario. In addition the mass of the ^{13}C pocket obtained in these simulations ($\lesssim 10^{-5} M_{\odot}$) is still a factor of 10 smaller than what is required to reproduce the observations.

The s-process nucleosynthesis in rotating AGB stars is very dependent on the value of the diffusion coefficient and on the duration over which this mixing is efficiently operating in the shear layer during the interpulse (Siess et al. 2004). Reduced mixing coefficients (by one or two orders of magnitude) and/or shorter periods of efficient mixing during the interpulse can save the s-process nucleosynthesis. A possible solution to this problem could stem from the neglected effects of the magnetic field. Indeed, in AGB stars shear is maximum at the base of the convective envelope, precisely where we expect the generation of magnetic fields by a dynamo process. In a more consistent picture including the magnetic fields, it is reasonable to think that the differential rotation will be reduced, which will decrease the diffusion coefficient during the interpulse and thus reinforce the efficiency of the s-process. Recent studies including magnetic fields in stellar evolution calculations of massive stars attest of a noticeable deceleration of the central layers and the forcing of solid rotation in the core (Heger et al. 2003; Maeder & Meynet 2004).

2.4 *Some observational constraints and theoretical problems*

In this section, we limit our discussion to the intrinsic AGB stars, i.e. stars which are not part of a binary system, and we concentrate on spectroscopic observations of carbon, s-elements, fluorine, and lithium. Observationally, different classes of AGB stars can be identified, depending on their surface composition. Most of the AGB stars are of spectral class M, characteristic of giant stars in general, being deficient in ^{12}C (i.e. oxygen rich) and enriched in ^{14}N . S stars present overabundances of s-elements in their envelope such as Sr, Zr, Ba or Nd and the MS class is to be considered as intermediate between the S and M categories. Carbon-rich stars are characterized by a ratio $\text{C}/\text{O} > 1$ and, by opposition, oxygen-rich stars are those in which the observed $\text{C}/\text{O} < 1$. Here again, type SC represents an intermediate case between the S and C types. Finally, let us mention the existence of J stars which have a very low $^{13}\text{C}/^{12}\text{C} < 15$ and a higher C/O ratio

than M stars. Single stars are believed to evolve along the M-MS-S-SC-C sequence as a consequence of 3DUP, sharing a common relation of increasing s-process enhancement with increasing ^{12}C (Fig. 13) even if each group shows considerable scatter.

The 3DUP is the mechanism by which the elements synthesized in the thermal pulse can reach the stellar surface. Many observations attest of this phenomenon and the most obvious signature is the existence of carbon-rich stars. This spectral feature is naturally explained by the envelope enrichment with the ^{12}C produced in pulse. Observations of carbon stars show that their luminosity function¹⁵ varies significantly with metallicity (Mould & Aaronson 1986) and that the carbon overabundance is present in low-luminosity red giants, i.e. relatively young and low-mass AGB stars. This early carbon enrichment is a problem that stellar evolution calculations are facing for more than three decades, referred to as the “*carbon stars mystery*” (Iben 1981). The failure of current models to develop 3DUP episodes sufficiently early during the AGB evolution emphasizes our poor knowledge of the transport processes in stellar interiors. Simulations including diffusive overshooting at the base of the convective envelope (Blöcker et al. 2000) leads to a better agreement between modeling and observations, implicitly indicating the necessity to account for an additional source of mixing. An alternative approach to tackle this problem is to use synthetic AGB models. These computations aim at reproducing evolutionary features of AGB stars using a simplified description of stellar evolution which does not require the full and time consuming computations of their structural evolution. The description and recipes are derived from full

¹⁵The luminosity function represents the distribution (i.e., the number) of stars of various spectral types (or color) according to their brightness or luminosity.

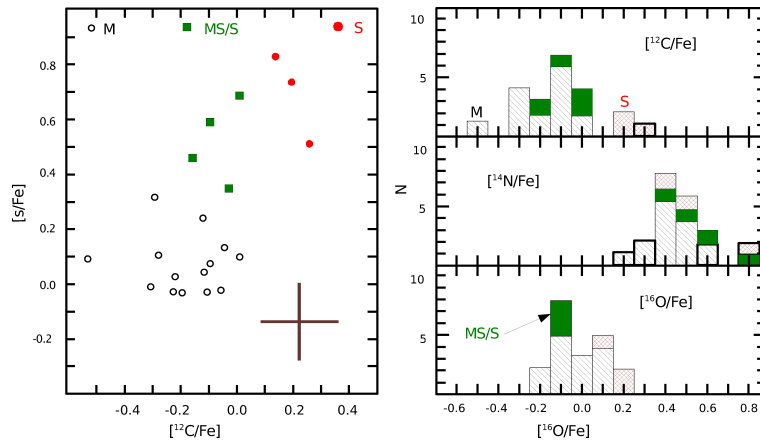


Fig. 13. Surface CNO abundances (left) and relationship between s-elements overabundances and ^{12}C for the different types of AGB stars (from Smith & Lambert 1986b).

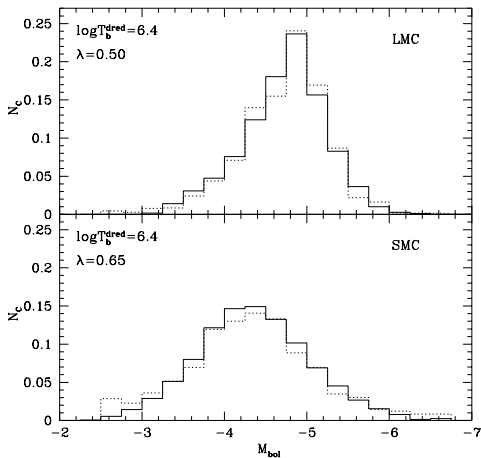


Fig. 14. Observational (solid line) and theoretical (dotted line) carbon star luminosity functions of the Small ($Z = 0.004$) and Large ($Z = 0.008$) Magellanic clouds (from Marigo et al. 1999)

evolutionary models or based on empirical relations (for details, see Groenewegen & Marigo 2003; Izzard et al. 2006). The power of these synthetic models lies on their speed and on their ability to explore the parameter space. For instance, one can modify the mass loss rate prescription, the nuclear reaction rates or the characteristics of the dredge-up and guess what would be the evolution and nucleosynthesis during the AGB phase. Using this indirect method, Marigo et al. (1999) was able to constrain the AGB parameters and reproduce the carbon star luminosity function of the Magellanic clouds (Fig. 14). These models show that for the SMC (LMC) the temperature at the base of the convective envelope at the time of the first thermal pulse must be of the order of 2.5×10^6 K (independently of the metallicity of these companion galaxies) and that the dredge up parameters $\lambda = 0.50$ (0.65). The result for λ is consistent with the theoretical expectation that the third dredge-up is more efficient at lower metallicities. Recent stellar models by Stancliffe et al. (2005) were able to reproduce the LMC distribution and their results agreed with the predictions of Marigo et al. (1999) concerning the envelope temperature, showing the good accuracy of these synthetic models. However, Stancliffe et al. (2005) could not reproduce at the same time the SMC carbon star luminosity function.

The detection by Merrill (1952) of the presence of technetium provided the first irrefutable proof that AGB stars are the site of the nucleosynthesis of s-elements. Indeed, Tc has unstable isotopes only¹⁶ with half-lives shorter than the duration of the AGB phase, so its presence clearly indicates that it was produced *in situ*. Thereafter, other s-elements were detected and a distinction was made between the light ones (*ls* for *light s*) including strontium (Sr), zirconium (Zr) and

¹⁶Technetium presents 3 long-lived isotopes, ^{97}Tc (half-life $\tau_{1/2} = 2.6 \times 10^6$ yr), ^{98}Tc ($\tau_{1/2} = 1.5 \times 10^6$ yr) and ^{99}Tc ($\tau_{1/2} = 2.1 \times 10^5$ yr)

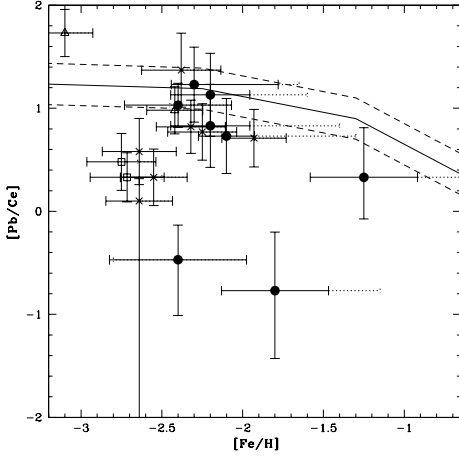


Fig. 15. Evolution of the $[Pb/Ce]$ ratio as a function of metallicity of some observed metal-poor stars. The solid line represents the theoretical prediction of the “partial mixing” models. The dashed lines delineate the uncertainties associated with this modeling (from Van Eck et al. 2003). The overshoot model is clearly unable to reproduce the spread in abundances at a given metallicity.

yttrium (y) and the heavy ones (hs for *heavy s*) like barium (Ba), lanthanum (La), neodymium (Nd) or samarium (Sm). Observations indicate a strong correlation between the abundances of carbon and s-elements (Busso et al. 1992; Lambert et al. 1995), clearly establishing that the s-process nucleosynthesis occurs in C-rich regions (see Sect. 2.3.3). In the recent years, much attention has been paid to the observation of very metal-poor stars (Van Eck et al. 2001; Aoki et al. 2001, 2002; Van Eck et al. 2003) which has led to the discovery of the so-called lead stars¹⁷. From a theoretical point of view, the detection of Pb was a great success of nucleosynthesis calculations. However, as mentioned before, a growing number of data do not conform to these predictions (Fig. 15). The problem may be related to the higher temperature found at the base of the envelope of metal-poor stars (Fig. 12).

In order to reproduce quantitatively the observed abundances of s-process elements at the surface of AGB stars, the mass of the proton mixing zone must be at least of $10^{-4} - 10^{-3} M_{\odot}$ (Straniero et al. 1995; Herwig 2000; Goriely & Mowlavi 2000). Such a large extent is hardly achieved by current stellar models and requires very high values of the overshooting parameter, typically $f_{\text{over}} \simeq 0.128$ (Lugaro et al. 2003). Alternatively, the gravity wave scenario seems to provide the natural conditions for the formation of a massive ^{13}C pocket (Denissenkov & Tout 2003). The radiative nucleosynthesis of s-elements during the interpulse also faces the problem of reproducing consistently the spread in s-abundances present among stars of similar mass and metallicity (Busso et al. 2001). This requires that the mass of the ^{13}C pocket changes from star to star. Maybe rotation plays a role but the problem remains open.

Fluorine constitutes a good tracer of the complex nucleosynthesis taking place

¹⁷As defined by $[Pb/hs] \gtrsim 1$, hs being any of Ba, La or Ce.

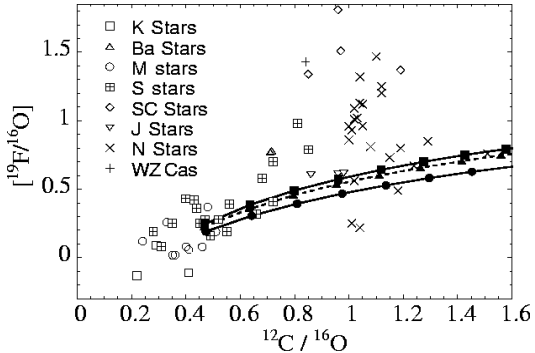


Fig. 16. Comparison of fluorine observations (Jorissen et al. 1992) with model predictions based on a $1.5 M_{\odot}$, $Z=0.018$ stellar model with overshooting. Each connected symbol corresponds to the enrichment due to a 3DUP episode. The two solid lines correspond to two different assumption for the dilution factors (for more details see Goriely & Mowlavi 2000, where this figure was taken)

in the pulse (see § 2.3). Statistically relevant abundance determinations of fluorine are still limited to nearby solar metallicity stars (Jorissen et al. 1992) but with the advent of instruments it is now possible to determine ^{19}F in the LMC and ω Centauri (Cunha et al. 2003) and in M4 (Smith et al. 2005). The sample of Jorissen et al. (1992) shows a strong correlation between fluorine on one hand and s-elements on the other hand. Current models reproduce these correlations (Mowlavi et al. 1996), but do not manage to account for the overabundance factors. In particular, the fluorine enhancement in the models is too small compared to that of carbon (Fig. 16). Including overshooting at the base of the convective envelope produces a larger ^{19}F enrichment leading to a better – but still not satisfactory – agreement with the observations. As a conclusion, the overshoot model reproduces quite well the correlation between fluorine and s-elements, but the fluorine and carbon enrichment, although correlated, quantitatively disagree with the data. This is still a major theoretical problem.

The discovery of Li-rich giants (Smith & Lambert 1990; Abia et al. 1991; Abia & Isern 1996; Smith et al. 1995) gave further credibility to the idea that HBB was actually occurring in massive AGB stars (Sackmann & Boothroyd 1992). However the efficiency of HBB is strongly dependent on the adopted treatment of convection (Sackmann & Boothroyd 1991; Ventura & D’Antona 2005). In particular, any modification to the treatment of heat transport in the convective regions (e.g. by changing the MLT parameter α or by using a different formalism for convection) modifies the temperature at the base of the envelope. The surface luminosity is directly affected (Fig. 17) and incidentally the mass loss rate and thus the duration of the AGB phase, the number of pulses and in the end the nucleosynthesis and the yields. As shown by Ventura & D’Antona (2005) in their study of a $5 M_{\odot}$ model, the theoretical surface abundances of CNO, ^{23}Na and ^{24}Mg can be significantly altered.

As a conclusion, from a theoretical point of view, the biggest problem that AGB modeling is facing is the treatment of mixing and in particular of convec-

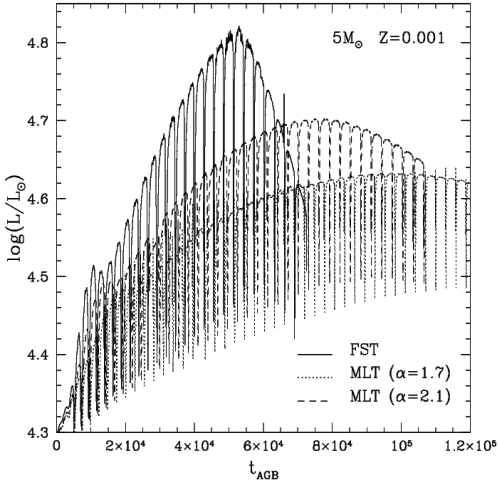


Fig. 17. Evolution of the surface luminosity of a $5 M_{\odot}$ model computed with different treatments of convection (from Ventura & D’Antona 2005)

tion. It is to be hoped that in the near future 3D hydrodynamical simulations (Dearborn et al. 2006; Eggleton et al. 2006; Herwig et al. 2006) will provide 1D stellar evolution code with a better description of the input physics.

3 Super-AGB stars

Massive stars evolve through all nuclear burning stages up to the formation of an iron core and then explode as core collapse supernovae (SNII, Ib or Ic). On the other hand, low- and intermediate-mass stars stop their nuclear evolution after He burning and end their life as degenerate CO white dwarfs after the expulsion of the envelope and the formation of a planetary nebula. Between these two regimes lie the super-AGB stars that ignite carbon but do not reach the minimum temperature for neon burning. They form oxygen-neon (ONe) core, that becomes degenerate and, similarly to AGB stars, they enter a thermally pulsing phase where the HeBS becomes recurrently unstable. Being more massive and composed of a ONe rather than a CO core, they are called super-AGB stars (hereafter SAGB stars).

In this section, we review their main evolutionary features, then describe their nucleosynthesis before addressing the question of their fate.

3.1 Carbon burning phase

The evolution of “massive AGB” stars prior to carbon ignition is very similar to that of lower mass stars. During the main sequence, the CNO cycle operates in a convective core and at H exhaustion, the 1DUP takes place. It leads to the same surface chemical modification as in intermediate-mass stars and, except for being more luminous, SAGB stars are chemically indistinguishable from standard RGB stars.

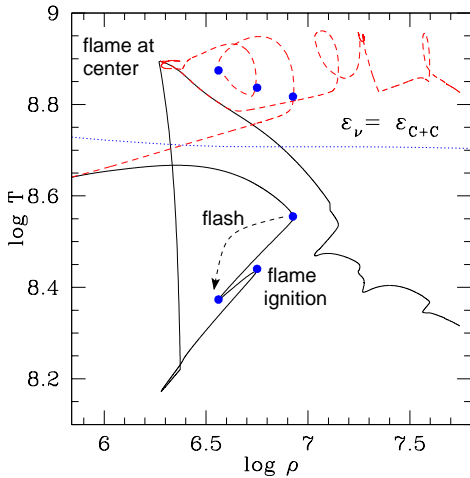


Fig. 18. Evolution in the $\rho - T$ plane of a representative $9.5 M_{\odot}$, $Z = Z_{\odot}$ model. The solid (dashed) line shows the evolution of the central (maximum, T_{\max}) temperature as a function of central density. The dotted line represents the locus of carbon ignition, i.e. when the nuclear energy production by C+C reactions overwhelms the neutrino energy losses. Below this line, carbon does not ignite.

At the end of helium burning, the increase in the central density boosts the neutrino emission and the temperature maximum (T_{\max}) moves outward. At the same time, gravitational energy flows from the contracting interior and the peak temperature increases. Eventually T_{\max} reaches $\sim 7 \times 10^8 \text{K}$ and carbon ignites off-center. In lower mass stars the situation is different because the temperature increase is stopped by the re-activation of the HBS which decouples the evolution of the core from that of the envelope. Indeed, the energy produced by the HBS balances the radiative losses from the surface, isolating the interior that stops contracting and heating. As illustrated in Fig. 18, in SAGB stars, the maximum temperature crosses the carbon ignition line defined in the $\rho - T$ plane by $\epsilon_{\nu} = \epsilon_{\text{C+C}}$. Above that line, the nuclear energy production rate associated with C+C reactions exceeds the neutrino energy loss rate, and so carbon burning is possible (i.e. exothermic).

Carbon burning proceeds in two steps characterized by the development of a strong flash followed by the propagation of a deflagration front to the center (Fig. 19). At the carbon ignition point, the thermodynamical conditions are similar to those encountered in the core of low-mass stars prior to the He flash : the plasma is partially degenerate ($\eta \simeq 2 - 3$) and when energy is deposited (this time by the $^{12}\text{C} + ^{12}\text{C}$ reactions) the temperature increases but the structure does not react. Therefore heat accumulates, the temperature gradient increases and a convective flash develops. The luminosity associated with the flash can be as large as $10^7 L_{\odot}$ and the duration of the instability typically ranges between a few hundred to a few thousand years (for details, see Siess 2006). The released energy is mainly absorbed to lift the degeneracy and subsequently converted into mechanical work. The large expansion that ensues produces a cooling of the stellar core as shown by the decrease in T_c and ρ_c in Fig. 18 and quenches the nuclear energy production. Thereafter contraction resumes and the maximum temperature moves inward in layers where the degeneracy has been lifted and where fuel is abundant. At carbon

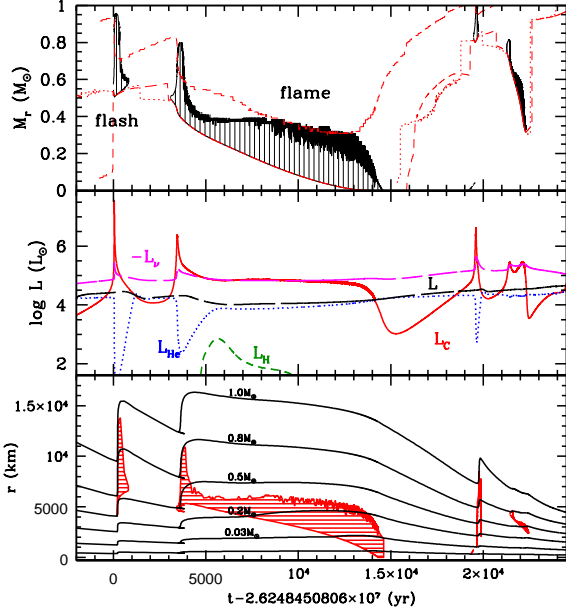


Fig. 19. Evolution of the internal structure of a $9.5 M_{\odot}$, $Z = Z_{\odot}$ model during central carbon burning. The lower and top panels are Kippenhahn diagrams in the eulerian and lagrangian representation, respectively. In the lower panel, the solid lines are iso-mass contours and illustrate the substantial expansion of the structure during the carbon flash and flame ignition. The mid-panel describes the evolution of the energetics in terms of the neutrino L_{ν} , hydrogen L_H , helium L_{He} and carbon L_C burning luminosities. The surface luminosity L remains almost unaffected by the nuclear burning operating in the core and during the flame propagation $L_C \simeq L_{\nu}$.

re-ignition, a second convective zone develops but the conditions are now different: first the degeneracy is lower ($\eta = 1$ compared to 2-3) and second, the convective zone develops in a region that was previously the site of carbon burning. It results that less fuel is available to power the instability and the peak carbon luminosity is significantly smaller¹⁸. Expansion is considerably reduced and is unable to quench nuclear burning. After a structural readjustment following the development of convection, a steady state is reached where all the energy produced by C-burning is instantaneously removed by the neutrinos. This can be seen in Fig. 19 by the almost perfect balance between L_{ν} and L_C . Under this balanced-power condition, carbon burning proceeds as a laminar deflagration (Timmes et al. 1994). A closer

¹⁸For carbon burning, the nuclear energy production is proportional to the square of the ^{12}C abundance.

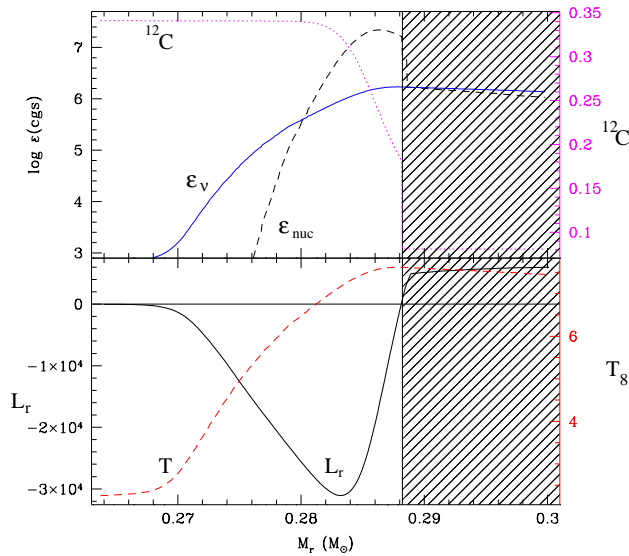


Fig. 20. Structure of the laminar flame. At the base of the convective flame (hatched area) the nuclear energy production rate (ϵ_{nuc}) is maximum. There, in the precursor flame, the luminosity profile (L_r) is negative. In the convective flame, the neutrino energy loss rate ϵ_ν is large and evacuates the energy deposited in the flame. The profiles of ^{12}C and temperature are also shown.

look at the energetics indicates that most of the nuclear energy is produced in a thin (a few km width) radiative region located just below the convective flame. There, the luminosity profile is negative indicating that energy flows toward the center (Fig. 20). This zone is referred to as the precursor flame and it is where carbon is nuclearly processed. As burning proceeds, the peak temperature moves inward (where the fuel is abundant) and the ashes of C-burning are engulfed in the convective flame. It should also be mentioned that in this steady C-burning phase, the stellar surface “does not feel” what is happening in its deep interior. After $10^4 - 10^5$ yr (depending on the initial stellar mass and metallicity) the flame reaches the center, convection disappears and C-burning proceeds in a shell. As can be seen from Fig. 19, this shell can occasionally meet some unburnt carbon pockets which leads to the formation of secondary C-burning convective zones.

3.2 Carbon nucleosynthesis and core composition

At carbon ignition, the core is mainly composed of ^{16}O ($\sim 63 - 73\%$), ^{12}C ($\sim 34 - 24\%$) with some remaining ^{22}Ne ($\lesssim 2\%$) produced earlier during core He burning. Carbon burning involves $^{12}\text{C}(^{12}\text{C},\alpha)^{20}\text{Ne}$ and $^{12}\text{C}(^{12}\text{C},\text{p})^{23}\text{Na}$ reactions mainly, followed in third place by $^{16}\text{O}(\alpha,\gamma)^{20}\text{Ne}$. These reactions transform the CO core into a ONe mixture and supply protons and α -particles for a richer nucleosynthesis.

In the carbon-burning zone, the α -particles that are not captured by ^{16}O react with ^{22}Ne and produce, via the (α,n) and (α,p) channels, the heavy $^{25,26}\text{Mg}$ isotopes plus some neutrons. These neutrons are then captured by the abundant ^{16}O and to a lower extent by ^{20}Ne , ^{23}Na and ^{25}Mg , leading the production of ^{17}O ,

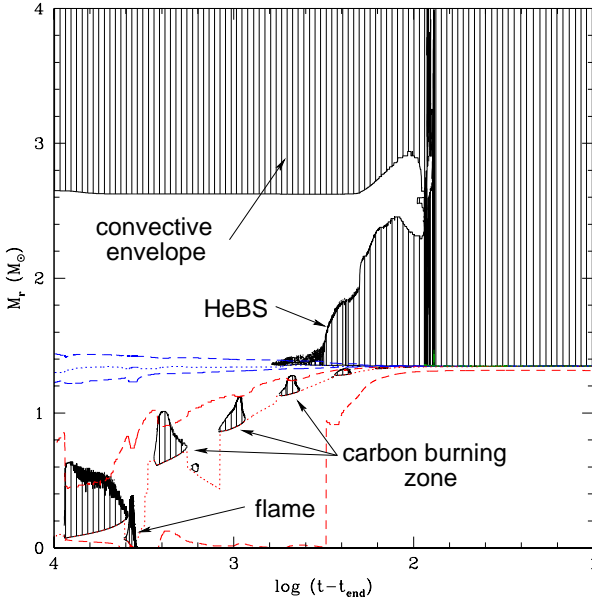


Fig. 21. Dredge-out phenomenon taking place in a $10.8 M_{\odot}$ star of solar composition. During this event, the convective zone that develops in the helium burning shell (HeBS) grows in mass and merges with the envelope. As a result, the H-depleted core mass moves from $\sim 2.62 M_{\odot}$ to $\sim 1.36 M_{\odot}$. In the x-axis, the time (in yr) is counted from the last model computed (t_{end}).

^{21}Ne , ^{24}Mg and ^{26}Mg . The protons mainly released by $^{12}\text{C}(^{12}\text{C},\text{p})^{23}\text{Na}$ contribute to the production of ^{20}Ne and ^{24}Mg by (p,α) and (p,γ) reactions on ^{23}Na , and to the synthesis of ^{27}Al by (p,γ) reactions on ^{26}Mg . After the passage of the flame, the ashes are essentially made of ^{16}O ($\sim 55 - 60\%$), ^{20}Ne ($\sim 28 - 32\%$), ^{23}Na ($\sim 5.5\%$), ^{24}Mg ($\sim 3.3\%$) and ^{25}Mg ($\sim 1.5\%$).

3.3 The second dredge-up

The second dredge-up is an important event in the evolution of SAGB stars, not only because it modifies their surface composition, but also because it can potentially hamper the formation of a supernova by reducing the size of the H depleted core below the Chandrasekhar mass. Depending on the initial stellar mass, the second dredge-up (2DUP) can take place before, during or after carbon burning (for details see Garcia-Berro et al. 1997; Siess 2006) or not at all as in massive stars. The occurrence of this deep mixing event is mostly related to evolutionary timescales. Lower mass stars evolve more slowly and the envelope penetration can take place before carbon ignites. Massive stars on the contrary avoid the 2DUP and evolve through all nuclear burning stages. An interesting evolutionary feature taking place in the upper mass range of the SAGB stars is the occurrence of the so-called dredge-out phenomenon (Iben et al. 1997; Siess & Pumo 2006). In this process (Fig. 21), a convective zone develops in the HeBS, grows in mass and merges with the envelope. The main consequences of this phenomenon are (1) a strong surface enrichment in ^{12}C and ^4He and (2) the reduction of the H-depleted core below the Chandrasekhar mass.

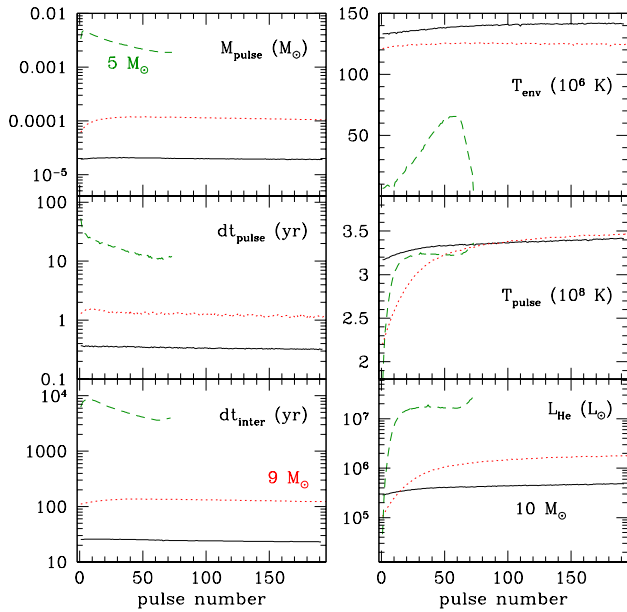


Fig. 22. Selected properties of the thermally pulsing phase of a $5 M_{\odot}$ (dashed line), $9 M_{\odot}$ (dotted line) and $10 M_{\odot}$ (solid line) as a function of pulse number for stars with a metallicity $Z = 0.004$. The quantities shown are the pulse mass (M_{pulse}) and duration (dt_{pulse}), interpulse period (dt_{inter}), maximum He luminosity during the pulse (L_{He}), maximum pulse temperature (T_{pulse}) and mean interpulse temperature at the base of the envelope (T_6^{env} in unit of 10^6K).

3.4 Thermally pulsing super-AGB phase

At the end of carbon burning, the contracting ONe core cools and becomes degenerate as a result of neutrino emission. The structure of the star is then similar to that of a standard AGB star : a nuclearily inert central core, surrounded by active He and H burning shells enshrouded in an extended convective envelope. There are however two fundamental differences with respect to AGB stars : first, the burning shells surround a much more massive core made of oxygen and neon rather than carbon and oxygen and second, the envelop mass is also significantly larger in super-AGB stars. These differences will strongly influence the fate of the star.

As for AGB stars, the He-burning shell is episodically unstable leading to the development of thermal pulses. Because of a larger core and envelope mass, the interpulse period is very short (a few hundred years for $9 M_{\odot}$ compared to $\gtrsim 10^4 \text{yr}$ for “standard” AGB stars). This implies that the SAGB stars will suffer a great number of thermal pulses, maybe as large as a few thousands. The pulse intensity – as measured by the He luminosity L_{He} – is much weaker in SAGB stars and the pulse duration is also considerably shorter than in AGB stars. The main reason for this behavior comes from the fact that, the structure being hotter, the contribution of the radiative pressure to the total pressure is larger. Since $P_{\text{rad}} \propto T^4$, a small temperature increase will induce a large over-pressure which will force the structure to readjust quickly. In these circumstances, less energy can accumulate and the instability is therefore less violent. Due to the stronger gravitational pull, the mass of the convective pulse is very small (at most a few $10^{-4} M_{\odot}$ which is one or

two orders of magnitude smaller than in AGB stars) and the temperature at its base is very high ($T_{\text{pulse}} \gtrsim 3.2 \times 10^8 \text{K}$) allowing for an efficient release of neutrons by the $^{22}\text{Ne}(\alpha, n)$ reactions. Very high temperatures can also be achieved at the base of the convective envelope (up to $T_{\text{env}} \gtrsim 1.5 \times 10^8 \text{K}$) which leads to a very efficient HBB and substantial modification of the envelope composition. Figure 22 illustrates and compares some of the properties of the SAGB *vs* AGB stars.

3.5 Nucleosynthesis

The nucleosynthesis inside the pulse remains essentially the same as in AGB stars. The most noticeable difference comes from the faster rate of the $^{22}\text{Ne}(\alpha, n)$ reactions which leads to an increased production of ^{25}Mg . The hotter environment also favors the destruction of fluorine by $^{19}\text{F}(\alpha, p)^{22}\text{Ne}$ and $^{19}\text{F}(n, \gamma)$. The released neutrons also participate to the s-process nucleosynthesis and to the enhancement of the ^{17}O abundance.

But the most noticeable chemical signature of SAGB stars results from the action of HBB (Fig. 23). Proton burning at the base of the convective envelope leads to a decrease in ^{12}C and ^{13}C to the benefit of ^{14}N , bringing the $^{12}\text{C}/^{13}\text{C}$ and C/N ratios to their equilibrium values of ~ 4 and $\sim 10^{-2}$, respectively. The activation of the ON-cycle contributes to oxygen depletion increasing the C/O ratio, but maintaining the star oxygen-rich. At $1.2 \times 10^8 \text{K}$, the neon isotopes (^{20}Ne and ^{22}Ne mainly) and ^{23}Na cannot survive and the NeNa-chain does not cycle anymore; instead a strong leakage to the MgAl-chain takes place. In these conditions, ^{24}Mg is also burnt to the benefit of the heavier magnesium isotopes ($^{25,26}\text{Mg}$), ^{27}Al and more spectacularly of the radio-active ^{26}Al ¹⁹. Any leakage out of the MgAl chain via $^{27}\text{Al}(p, \gamma)^{28}\text{Si}$ is extremely weak (Arnould et al. 1999) so the abundance of elements with $A > 27$ remains almost unchanged.

As a consequence of HBB, super AGB stars are expected to be strong producers of ^{14}N , $^{25,26}\text{Mg}$ and $^{26,27}\text{Al}$. The chemical effects of the 3DUP episodes on the surface composition remain relatively small. Indeed, the pulse mass (at most $10^{-4} M_{\odot}$) is almost six orders of magnitude smaller than the envelope mass ($\sim 10 M_{\odot}$), making the 3DUP very inefficient in polluting the surface. In comparison, the dilution factor in an AGB star is of the order of 10^{-3} ! So it is safe to say that the presence of the 3DUP episodes in SAGB stars will not affect substantially the surface composition. The burning of the envelope by HBB will mainly determine the yields.

3.6 The initial mass range and fate of SAGB stars

The initial mass of SAGB stars ranges between a lower limit, usually referred to as M_{up} , and an upper limit defined as M_{mas} . Stars less massive than M_{up} do not ignite carbon and evolve through the thermally pulsing AGB phase where they synthesize many important elements, such as C, N and the heavy s-elements,

¹⁹Note that the half life of ^{26}Al , $7.2 \times 10^5 \text{yr}$, is longer than the entire SAGB phase.

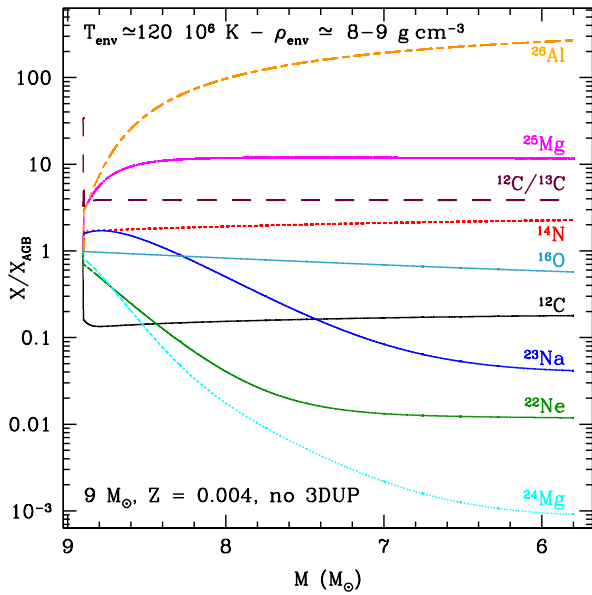


Fig. 23. Evolution of the surface abundance in a $9 M_{\odot}$, $Z = 0.004$ model where the temperature at the base of the convective envelope is $T_{\text{env}} \simeq 1.2 \times 10^8 \text{K}$. The abundances are scaled to their value at the beginning of the TP-SAGB phase. Consequently, the effects of the first and second dredge-ups do not appear here.

ending their lives as planetary nebulae and CO white dwarfs. Stars more massive than M_{mas} ignite carbon centrally and avoid the AGB phase. These “massive stars” will end their lives as core collapse Supernovae. The values of M_{up} and M_{mas} depend on the initial chemical composition and on the amount of mixing at the edge of the convective cores (Siess 2007). As illustrated in Fig. 24, these transition masses decrease with Z and reach a minimum around $Z \simeq 10^{-4}$. The reason for this behavior comes from the fact that at lower metallicities, because of the reduced envelope opacity and higher luminosity, stars develop more massive cores in order to provide the energy necessary to power the surface luminosity. They thus behave as more massive stars and are able to ignite carbon at a lower initial mass, explaining why M_{up} and M_{mas} decrease with Z (Fig. 24). Below $Z \simeq 10^{-4}$, M_{up} and M_{mas} start to increase again because of the stronger contribution of the pp-chain to the overall energy production in these metal-poor stars (Tornambe & Chieffi 1986). Finally it is important to note that these limiting masses are very sensitive to additional mixing. For example, computations including a moderate overshooting at the edge of the convective core will lower M_{up} and M_{mas} by almost $2 M_{\odot}$!

As the star evolves on the TP-SAGB, the core grows as a result of shell burning and may reach the critical mass of $1.37 M_{\odot}$ (Nomoto 1984) corresponding to the Chandrasekhar limit, which marks the beginning of core collapse. When this limit is reached, the density in the core is high enough so that the electron Fermi energy becomes larger than the threshold energy for electron capture reactions. In these circumstances, electron capture reactions start on ^{24}Mg and proceed up to the abundant ^{20}Ne (Ritossa et al. 1999). The resulting decrease in electron

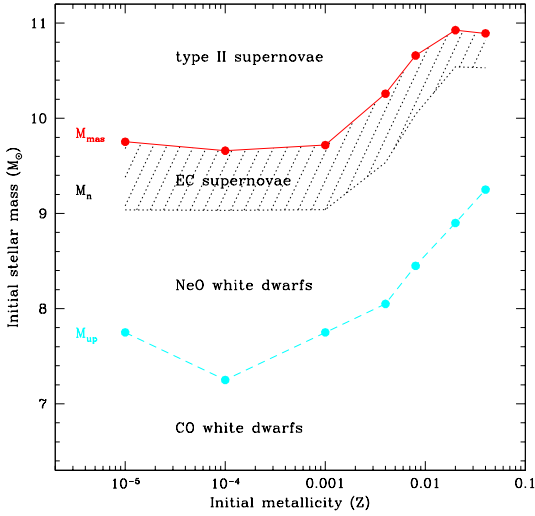


Fig. 24. Mass transitions for models without core overshooting as a function of initial metallicity. Stars with initial mass less than M_{up} will not ignite carbon and leave a CO white dwarf. Between M_{up} and M_{n} , the remnant is a ONe white dwarf. Inside the shaded area, depending on the adopted values for the core growth and mass loss rates, the SAGB star can evolve toward electron capture supernovae. Stars with mass larger than M_{mas} behave as massive stars and end their life as iron core collapse SN (for more details, see Siess 2007).

number density (Y_e) has important consequences : (1) it reduces the electron pressure so core contraction is accelerated²⁰ (2) the Chandrasekhar mass (which is proportional to Y_e^2) decreases so core collapse is additionally facilitated and (3) the heating by γ -ray emission from the electron capture reactions can ignite neon and oxygen burning (Miyaji et al. 1980; Nomoto 1987). In this last and poorly studied stage of the evolution, convection can develop in the region of electron captures leading to the activation of the URCA process (Ritossa et al. 1999).

At the end of the collapse, a neutron star will form. This scenario, referred to as electron-capture core collapse supernova (EC-SN), is supposed to be at the origin of the formation of low-mass neutrons stars, and is a possible site for the “r-process” nucleosynthesis when the shock wave, generated when the collapsing layers bounce on the newly formed neutron star, crosses the neon rich layers and activates the ^{22}Ne neutron source.

The minimum mass for a star to follow the EC-SN scenario is referred to as M_{n} , and is critically dependent on the mass loss (\dot{M}_{wind}) and core growth (\dot{M}_{core}) rates (Siess 2007; Poelarends et al. 2007). If the mass loss is large enough, the envelop is lost before the core mass reaches $1.37M_{\odot}$ and the evolutionary endpoint is a ONe white dwarf. On the contrary the EC-SN explosion is inevitable. These two quantities (\dot{M}_{wind} and \dot{M}_{core}) are unfortunately badly constrained. The case of SAGB is particularly ambiguous since no specific mass loss rate prescription is available, the realistic value ranging between the usual AGB and massive star rates. For a typical SAGB star of $\sim 10^5 L_{\odot}$, $\sim 1200 R_{\odot}$ and with $T_{\text{eff}} \simeq 3000$ K, using different mass loss rates prescriptions gives $1.5 \times 10^{-4} M_{\odot}\text{yr}^{-1}$ with Vassiliadis

²⁰The situation is even worse because as the density increases the electron Fermi energy also increases so that the electron capture reaction rates become even larger.

& Wood (1993), $8.5 \times 10^{-3} M_{\odot} \text{yr}^{-1}$ with Bloeker (1995) or $5.3 \times 10^{-6} M_{\odot} \text{yr}^{-1}$ with the de Jager et al. (1988) rate for massive stars. Concerning the core growth rate, this value is also subject to large uncertainties mainly associated with the amplitude of the 3DUP. For instance, if the dredge-up is very efficient, λ (Eq. 2.1) is close to one and the core mass does not increase from pulse to pulse. These uncertainties affect the determination of M_n which value ranges in the shaded area of Fig. 24.

These results show that the mass range for EC-SN is extremely small, ranging between 10.6 and 11 M_{\odot} at solar metallicity so only a small fraction of SAGB stars will follow this evolutionary path. It should also be emphasized that at lower metallicity, these SN explosions were much more numerous since they were produced by lower mass stars. And as a conclusion, given the properties of the IMF, we may expect that the progenitors of a large fraction of type II SN be SAGB stars.

References

- Abia, C., Boffin, H. M. J., Isern, J., & Rebolo, R. 1991, *A&A*, 245, L1
- Abia, C. & Isern, J. 1996, *ApJ*, 460, 443
- Aoki, W., Norris, J. E., Ryan, S. G., Beers, T. C., & Ando, H. 2000, *ApJ Letters*, 536, L97
- Aoki, W., Ryan, S. G., Norris, J. E., et al. 2001, *ApJ*, 561, 346
- Aoki, W., Ryan, S. G., Norris, J. E., et al. 2002, *ApJ*, 580, 1149
- Aoki, W., Ryan, S. G., Tsangarides, S., et al. 2003, *Elemental Abundances in Old Stars and Damped Lyman- α Systems*, 25th meeting of the IAU, Joint Discussion 15, 22 July 2003, Sydney, Australia, 15
- Arnould, M., Goriely, S., & Jorissen, A. 1999, *A&A*, 347, 572
- Blöcker, T., Herwig, F., Schönberner, D., & El Eid, M. 2000, in *IAU Symposium*, 524
- Bloeker, T. 1995, *A&A*, 297, 727
- Boothroyd, A. I. & Sackmann, I.-J. 1988a, *ApJ*, 328, 653
- Boothroyd, A. I. & Sackmann, I.-J. 1988b, *ApJ*, 328, 671
- Briley, M. M., Cohen, J. G., & Stetson, P. B. 2004a, *AJ*, 127, 1579
- Briley, M. M., Harbeck, D., Smith, G. H., & Grebel, E. K. 2004b, *AJ*, 127, 1588
- Burbidge, E. M., Burbidge, G. R., Fowler, W. A., & Hoyle, F. 1957, *Reviews of Modern Physics*, 29, 547
- Busso, M., Gallino, R., Lambert, D. L., Raiteri, C. M., & Smith, V. V. 1992, *ApJ*, 399, 218
- Busso, M., Gallino, R., Lambert, D. L., Travaglio, C., & Smith, V. V. 2001, *ApJ*, 557, 802
- Cameron, A. G. W. & Fowler, W. A. 1971, *ApJ*, 164, 111
- Carretta, E., Gratton, R. G., Bragaglia, A., Bonifacio, P., & Pasquini, L. 2004, *A&A*, 416, 925

- Charbonnel, C. 1995, *ApJ Letters*, 453, L41
- Charbonnel, C. & Do Nascimento, J. D. 1998, *A&A*, 336, 915
- Charbonnel, C. & Zahn, J.-P. 2007, *A&A*, 467, L15
- Clayton, D. D., Fowler, W. A., Hull, T. E., & Zimmerman, B. A. 1961, *Annals of Physics*, 12, 331
- Cunha, K., Smith, V. V., Lambert, D. L., & Hinkle, K. H. 2003, *AJ*, 126, 1305
- Da Costa, G. S., Cannon, R., Croke, B., & Norris, J. 2004, *Mem. Soc. Astr. It.*, 75, 370
- de Jager, C., Nieuwenhuijzen, H., & van der Hucht, K. A. 1988, *A&AS*, 72, 259
- Dearborn, D. S. P., Lattanzio, J. C., & Eggleton, P. P. 2006, *ApJ*, 639, 405
- Decressin, T. 2007, Ph.D. Thesis
- Denissenkov, P. A., Da Costa, G. S., Norris, J. E., & Weiss, A. 1998, *A&A*, 333, 926
- Denissenkov, P. A. & Tout, C. A. 2000, *MNRAS*, 316, 395
- Denissenkov, P. A. & Tout, C. A. 2003, *MNRAS*, 340, 722
- Denissenkov, P. A. & Vandenberg, D. A. 2003, *ApJ*, 593, 509
- Denissenkov, P. A. & Weiss, A. 1996, *A&A*, 308, 773
- Despain, K. H. 1981, *ApJ*, 251, 639
- Deupree, R. G. 1996, *ApJ*, 471, 377
- Eggleton, P. P., Dearborn, D. S. P., & Lattanzio, J. C. 2006, *Science*, 314, 1580
- Freytag, B., Ludwig, H.-G., & Steffen, M. 1996, *A&A*, 313, 497
- Frogel, J. A., Mould, J., & Blanco, V. M. 1990, *ApJ*, 352, 96
- Frost, C. A. & Lattanzio, J. C. 1996, *ApJ*, 473, 383
- Gallino, R., Arlandini, C., Busso, M., et al. 1998, *ApJ*, 497, 388
- Garcia-Berro, E., Ritossa, C., & Iben, I. J. 1997, *ApJ*, 485, 765
- Goriely, S. & Mowlavi, N. 2000, *A&A*, 362, 599
- Goriely, S. & Siess, L. 2001, *A&A*, 378, L25
- Goriely, S. & Siess, L. 2004, *A&A*, 421, L25
- Gratton, R. G., Bonifacio, P., Bragaglia, A., et al. 2001, *A&A*, 369, 87
- Gratton, R. G., Sneden, C., Carretta, E., & Bragaglia, A. 2000, *A&A*, 354, 169
- Groenewegen, M. A. T. & Marigo, P. 2003, in *Asymptotic giant branch stars*, by Harm J. Habing and Hans Olofsson. *Astronomy and astrophysics library*, New York, Berlin: Springer, 2003, ed. H. J. Habing & H. Olofsson, 105–148
- Heger, A., Woosley, S. E., & Langer, N. 2003, in *IAU Symposium*, 357
- Herwig, F. 2000, *A&A*, 360, 952
- Herwig, F., Blöcker, T., & Schönberner, D. 1999, in *IAU Symp. 191: Asymptotic Giant Branch Stars*, 41
- Herwig, F., Bloeker, T., Schönberner, D., & El Eid, M. 1997, *A&A*, 324, L81
- Herwig, F., Freytag, B., Hueckstaedt, R. M., & Timmes, F. X. 2006, *ApJ*, 642, 1057

- Herwig, F., Langer, N., & Lugaro, M. 2003, *ApJ*, 593, 1056
- Iben, I. 1981, *ApJ*, 246, 278
- Iben, I. & Renzini, A. 1982, *ApJ Letters*, 263, L23
- Iben, I. & Renzini, A. 1984, *Phys. Rep.*, 105, 329
- Iben, I. J., Ritossa, C., & Garcia-Berro, E. 1997, *ApJ*, 489, 772
- Imbriani, G., Limongi, M., Gialanella, L., et al. 2001, *ApJ*, 558, 903
- Ivans, I. I., Kraft, R. P., Sneden, C., et al. 2001, *AJ*, 122, 1438
- Izzard, R. G., Dray, L. M., Karakas, A. I., Lugaro, M., & Tout, C. A. 2006, *A&A*, 460, 565
- Jorissen, A., Smith, V. V., & Lambert, D. L. 1992, *A&A*, 261, 164
- Kappeler, F., Beer, H., & Wisshak, K. 1989, *Reports of Progress in Physics*, 52, 945
- Karakas, A. I., Lattanzio, J. C., & Pols, O. R. 2002, *PASA*, 19, 515
- Lambert, D. L., Smith, V. V., Busso, M., Gallino, R., & Straniero, O. 1995, *ApJ*, 450, 302
- Langer, N., Heger, A., Wellstein, S., & Herwig, F. 1999, *A&A*, 346, L37
- Lattanzio, J. C. 1989, *ApJ Letters*, 344, L25
- Lugaro, M., Herwig, F., Lattanzio, J. C., Gallino, R., & Straniero, O. 2003, *ApJ*, 586, 1305
- Maeder, A. & Meynet, G. 2004, *A&A*, 422, 225
- Marigo, P., Girardi, L., & Bressan, A. 1999, *A&A*, 344, 123
- McWilliam, A. & Lambert, D. L. 1988, *MNRAS*, 230, 573
- Mengel, J. & Sweigart, A. V. 1981, in *IAU Colloq. 68: Astrophysical Parameters for Globular Clusters*, 277
- Merrill, S. P. W. 1952, *ApJ*, 116, 21
- Miyaji, S., Nomoto, K., Yokoi, K., & Sugimoto, D. 1980, *PASJ*, 32, 303
- Mould, J. & Aaronson, M. 1986, *ApJ*, 303, 10
- Mowlavi, N. 1999, *A&A*, 344, 617
- Mowlavi, N., Jorissen, A., & Arnould, M. 1996, *A&A*, 311, 803
- Nomoto, K. 1984, *ApJ*, 277, 791
- Nomoto, K. 1987, *ApJ*, 322, 206
- Palacios, A., Charbonnel, C., Talon, S., & Siess, L. 2006, *A&A*, 453, 261
- Poelarends, A. J. T., Herwig, F., Langer, N., & Heger, A. 2007, *ApJ*, in press
- Pols, O. R. & Tout, C. A. 2001, *Mem. Soc. Astr. It.*, 72, 299
- Ramírez, S. V. & Cohen, J. G. 2002, *AJ*, 123, 3277
- Ritossa, C., García-Berro, E., & Iben, I. J. 1999, *ApJ*, 515, 381
- Sackmann, I.-J. & Boothroyd, A. I. 1991, *ApJ*, 366, 529
- Sackmann, I.-J. & Boothroyd, A. I. 1992, *ApJ Letters*, 392, L71
- Schwarzschild, M. & Härm, R. 1965, *ApJ*, 142, 855

- Siess, L. 2006, *A&A*, 448, 717
- Siess, L. 2007, *A&A*, 476, 893
- Siess, L. & Goriely, S. 2002, in SF2A-2002, EdP-Sciences, Conference Series, 567
- Siess, L. & Goriely, S. 2003, *Nucl. Phys. A*, 718, 524c
- Siess, L., Goriely, S., & Langer, N. 2003, *PASA*, 20, 371
- Siess, L., Goriely, S., & Langer, N. 2004, *A&A*, 415, 1089
- Siess, L., Livio, M., & Lattanzio, J. 2002, *ApJ*, 570, 329
- Siess, L. & Pumo, M. L. 2006, *Mem. Soc. Astr. It.*, 77, 822
- Smith, V. V., Cunha, K., Ivans, I. I., et al. 2005, *ApJ*, 633, 392
- Smith, V. V. & Lambert, D. L. 1986a, *ApJ*, 311, 843
- Smith, V. V. & Lambert, D. L. 1986b, *ApJ*, 311, 843
- Smith, V. V. & Lambert, D. L. 1990, *ApJ Letters*, 361, L69
- Smith, V. V., Plez, B., Lambert, D. L., & Lubowich, D. A. 1995, *ApJ*, 441, 735
- Snedden, C. 1999, *Astrophysics and Space Science*, 265, 145
- Snedden, C., Kraft, R. P., Guhathakurta, P., Peterson, R. C., & Fulbright, J. P. 2004, *AJ*, 127, 2162
- Stancliffe, R. J. 2006, *MNRAS*, 370, 1817
- Stancliffe, R. J., Izzard, R. G., & Tout, C. A. 2005, *MNRAS*, 356, L1
- Straniero, O., Chieffi, A., Limongi, M., et al. 1997, *ApJ*, 478, 332
- Straniero, O., Domínguez, I., Imbriani, G., & Piersanti, L. 2003, *ApJ*, 583, 878
- Straniero, O., Gallino, R., Busso, M., et al. 1995, *ApJ Letters*, 440, L85
- Sweigart, A. V. & Mengel, J. G. 1979, *ApJ*, 229, 624
- Thévenin, F., Charbonnel, C., de Freitas Pacheco, J. A., et al. 2001, *A&A*, 373, 905
- Timmes, F. X., Woosley, S. E., & Taam, R. E. 1994, *ApJ*, 420, 348
- Tornambe, A. & Chieffi, A. 1986, *MNRAS*, 220, 529
- Travaglio, C., Randich, S., Galli, D., et al. 2001, *ApJ*, 559, 909
- Van Eck, S., Goriely, S., Jorissen, A., & Plez, B. 2001, *Nature*, 412, 793
- Van Eck, S., Goriely, S., Jorissen, A., & Plez, B. 2003, *A&A*, 404, 291
- Vassiliadis, E. & Wood, P. R. 1993, *ApJ*, 413, 641
- Ventura, P. & D'Antona, F. 2005, *A&A*, 431, 279
- Wagenhuber, J. & Groenewegen, M. A. T. 1998, *A&A*, 340, 183
- Weiss, A., Denissenkov, P. A., & Charbonnel, C. 2000, *A&A*, 356, 181
- Wood, P. R. 1981, *ApJ*, 248, 311